STRUCTURAL CHEMISTRY

ISSN 2053-2296

3,4-Bis-*O*-propargyl-1,2:5,6-di-*O*-isopropylidene-D-mannitol: a study of multiple weak hydrogen bonds in the solid state

Adnan I. Mohammed,[a] Mohan M. Bhadbhade[b] and Roger W. Read[c]*

[a]Department of Chemistry, College of Science, University of Kerbala, Karbala, Iraq, [b]Mark Wainwright Analytical Centre, The University of New South Wales (UNSW), Sydney, NSW 2052, Australia, and [c]School of Chemistry, The University of New South Wales (UNSW), Sydney, NSW 2052, Australia. *Correspondence e-mail: r.read@unsw.edu.au

Received 16 March 2022
Accepted 7 September 2022

Edited by S. Moggach, The University of Western Australia, Australia

Keywords: chemical crystallography; weak hydrogen bonds; noncovalent interactions; crystal structure; crystal engineering; supramolecular chemistry; CSD.

CCDC reference: 2055328

Supporting information: this article has supporting information at journals.iucr.org/c

The title homochiral compound, $C_{18}H_{26}O_6$, **1**, was examined by single-crystal X-ray crystallography in order to understand its potential as a synthetic building block, particularly in inter- and intramolecular cyclocondensation reactions. It has also proven to be an excellent model for understanding multiple weak donor–acceptor D—H···A interactions involving terminal acetylenes as donors and as acceptors. The asymmetric unit of **1** comprises three almost identical independent molecules, each with the mannitol 2*R*,3*R*,4*R*,5*R* configuration and different conformations. Like independent molecules align in strands through acetylenic donor C—H···O contacts with equivalent dioxolanyl acceptor groups. Two of the strands are aligned unidirectionally, in parallel, while the third strand aligns perpendicular to the first two, to give interwoven layers in the supramolecular structure. A detailed study of the interdigitation of the second propargyl group from each independent molecule between strands, and of other short interstrand C—H···O contacts, provides new insight into the application of weak hydrogen-bond theory within the context of a conformationally flexible symmetrical molecule. Analyses of the Cambridge Structural Database using Crystal Packing Features and *ConQuest* search motifs support the importance of the D···A distance parameter, demonstrate the different influences of donor and acceptor types, and reveal the interplay between H···A and D···A contributions in different contact types.

1. Introduction

Propargyl groups are small and can serve as protection for alcohols that can be selectively removed in the presence of acetonides (1,3-dioxolanyls), methoxymethyl (MOM), benzyl and *tert*-butyldimethylsilyl (TBS) ethers (Manabe *et al.*, 2008; Rambabu *et al.*, 2013), and provide subtle enhancement of diastereoselectivity in the synthesis of β-mannopyranosylated disaccharides (Crich *et al.*, 2006). Propargyloxy groups can also undergo a variety of useful transformations in their own right. One of us recently described the synthesis of 3,4-bis-*O*-propargyl-1,2:5,6-di-*O*-isopropylidene-D-mannitol, **1**, and its use in Cu^I-catalyzed dipolar cycloaddition reactions with *n*-alkyl azides to generate model compounds for potential new gemini surfactants (Mohammed *et al.*, 2012), and extended this study in a collaborative effort to *O*-propargyl derivatives of glucose and galactose sugars and their reactions with polyfluoroalkyl azides as a route to novel fluorous surfactants (Ahmed *et al.*, 2020). Related sugar-derived oligo-propargyl ethers have participated in intramolecular 1,3-dipolar nitrone addition (Ghorai *et al.*, 2005) and been used as versatile building blocks in diversity-oriented synthesis of macrocycles (Maurya & Rana, 2017), while oligo-propargylated sugars and other polyols have been used with oligoazides in a modular

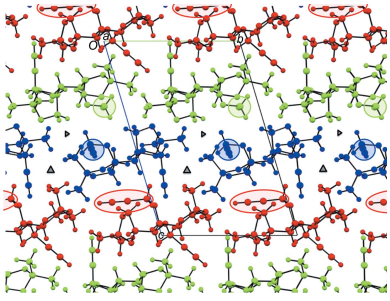

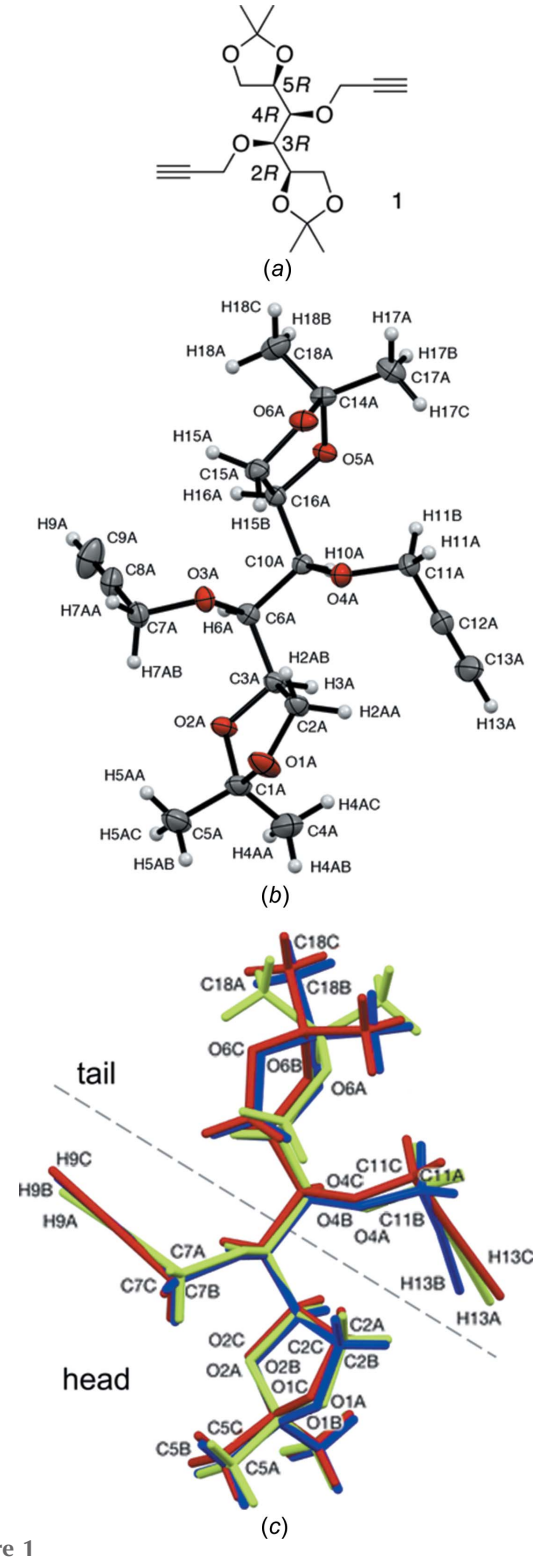

Figure 1
(*a*) The molecular structure of title compound **1**, showing the mannitol 2*R*,3*R*,4*R*,5*R* configuration. (*b*) The molecular structure of molecule *A*, showing the crystallographic atom-numbering scheme used throughout the remainder of the discussion, with displacement ellipsoids drawn with *Mercury CSD* (Version 3.0; Macrae *et al.*, 2020) at the 40% probability level and H atoms shown as small spheres of arbitrary radius. (*c*) Overlay of molecules *A* (green), *B* (blue) and *C* (red) from the unit cell of compound **1** represented in capped sticks format, showing good overlap in the O1/O2 dioxolanyl portion (head) and significant variation, especially by molecule *A*, in the O5/O6 dioxolanyl portion (tail).

Table 1
Experimental details.

Crystal data	
Chemical formula	$C_{18}H_{26}O_6$
M_r	338.39
Crystal system, space group	Triclinic, *P*1
Temperature (K)	150
a, *b*, *c* (Å)	9.4726 (4), 10.3000 (5), 15.3583 (7)
α, β, γ (°)	73.378 (2), 88.382 (2), 86.400 (2)
V (Å^3)	1432.94 (11)
Z	3
Radiation type	Mo *K*α
μ (mm^{-1})	0.09
Crystal size (mm)	0.24 × 0.21 × 0.19
Data collection	
Diffractometer	Bruker APEXII CCD
Absorption correction	Multi-scan (*SADABS*; Bruker, 2016)
T_{min}, T_{max}	0.679, 0.746
No. of measured, independent and observed [$I > 2\sigma(I)$] reflections	25389, 8343, 8134
R_{int}	0.028
(sin $\theta/\lambda)_{max}$ (Å^{-1})	0.595
Refinement	
$R[F^2 > 2\sigma(F^2)]$, $wR(F^2)$, *S*	0.026, 0.065, 1.02
No. of reflections	8343
No. of parameters	661
No. of restraints	3
H-atom treatment	H-atom parameters constrained
$\Delta\rho_{max}$, $\Delta\rho_{min}$ (e Å^{-3})	0.21, −0.15
Absolute structure	Flack *x* determined using 3228 quotients $[(I^+) - (I^-)]/[(I^+) + (I^-)]$ (Parsons *et al.*, 2013)
Absolute structure parameter	0.04 (17)

Computer programs: *APEX3* (Bruker, 2016), *SAINT* (Bruker, 2016), *SHELXT* (Sheldrick, 2015*a*), *SHELXL* (Sheldrick, 2015*b*) and *OLEX2* (Dolomanov *et al.*, 2009).

approach to neoglycoconjugates (Perez-Baldaras *et al.*, 2009). Similar vicinal propargyl ethers derived from furfural have found use in conversion to bisphenols (Hashmi *et al.*, 2007). Furthermore, dipropargyl malonate and terephthalate esters generate di- and tetranuclear clusters with cobalt, molybdenum and ruthenium metal ions (Zhang *et al.*, 2001). In more tangential, although not exclusive, applications, cycloaddition reactions of bridged diacetylenic compounds have been used to generate a wide range of benzenoid substances, including fluoranthenes and indenocorannulenes (Wu *et al.*, 2006), and propargylic enediyne alcohols have shown participation in nucleophilic cycloaromatization (Poloukhtine *et al.*, 2010) akin to the important Bergman cyclization (Bergman, 1973). Relevant to these topics has been the lengthy and sometimes vexed discourse in the literature over the nature of C—H···O hydrogen bonds in crystals (Bernstein, 2013), where often the donor interactions of terminal acetylenic groups have been quoted. Matters of contention have been the acid strength and linearity of C—H···O hydrogen bonds (Desiraju, 1990, 1991), the distinction between weak attractive hydrogen bonds *versus* repulsive van der Waals interactions (Steiner & Desiraju, 1998, 1999; Schwalbe, 2012) and the attribution of contacts to electrostatics compared with van der Waals interactions (Steiner, 2002; Desiraju, 2002). Controversy over such matters has subsided (Bernstein, 2013), with an acceptance that in the solid state there is a continuum of these factors in

play, and the best measure of weak donor–acceptor D—H$\cdots A$ contact effectiveness is the $D\cdots A$ distance (D). Such considerations have influenced subsequent applications of weak hydrogen bonds to molecular recognition in organic crystals (Dunitz & Gavezzotti, 2005), virtual screening in drug design (Desiraju, 2005; Jones *et al.*, 2012) and crystal engineering (Desiraju, 2013, Baillargeon *et al.*, 2014).

As a homochiral vicinal bis-propargyl ether, substance **1** [Fig. 1(*a*)] therefore has potential to serve as a precursor for a wide range of intriguing materials whose function would depend largely upon tertiary structure and intermolecular interactions. Its solid-state structure also holds interest because of the close proximity of two notionally equivalent terminal acetylenic groups in the presence of two ethereal oxygen types (propargyloxy and dioxolanyl) as acceptors. The molecule was reprepared here and examined for the first time by single-crystal X-ray diffraction to ascertain a baseline for these structural features in the solid state.

2. Experimental

2.1. Synthesis

The synthesis of 3,4-bis-*O*-propargyl-1,2:5,6-di-*O*-isopropylidene-D-mannitol, **1** {systematic name: (1*R*,2*R*)-1,2-bis[(*R*)-2,2-dimethyl-1,3-dioxolan-4-yl]-1,2-bis(prop-2-yn-1-yloxy)ethane},

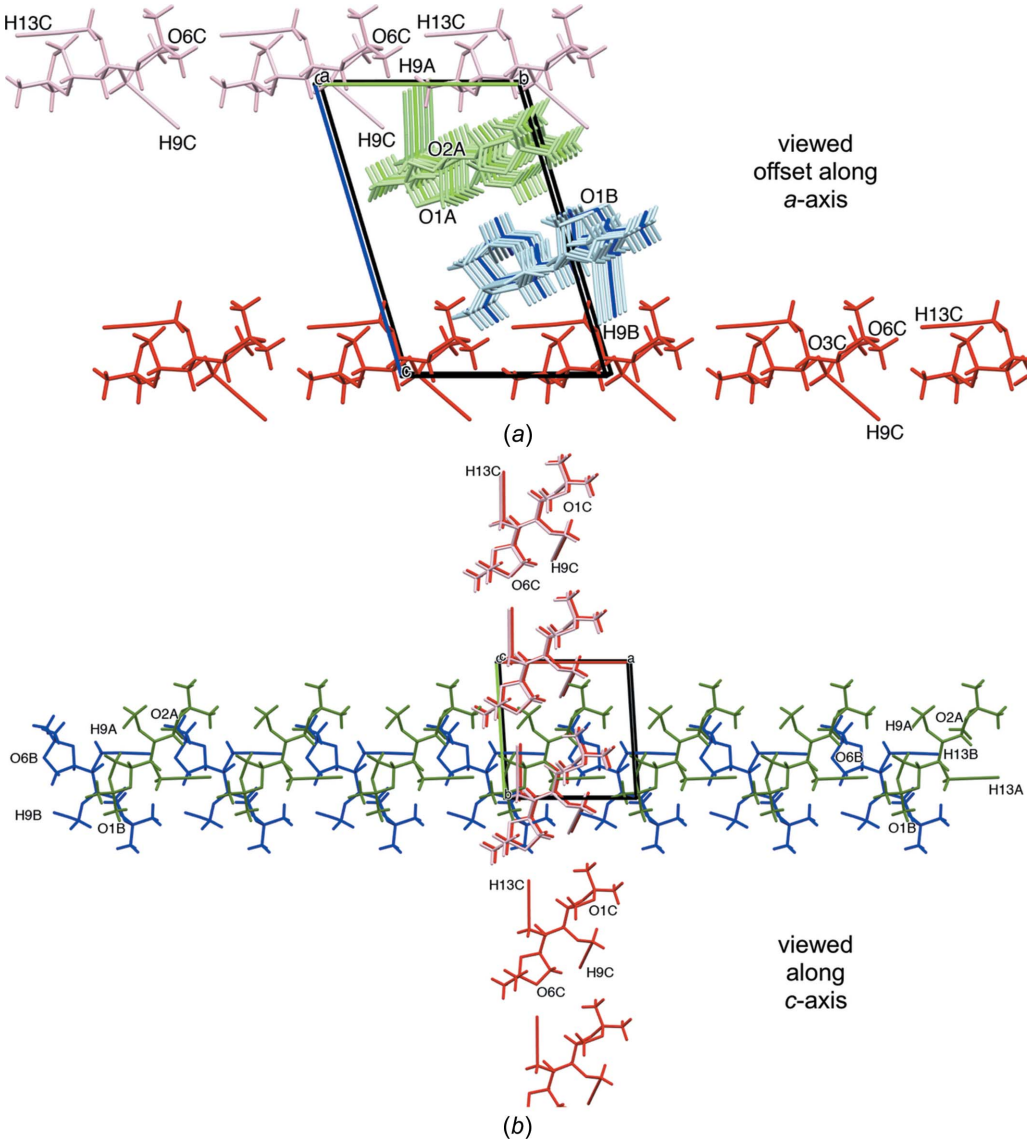

Figure 2
Individual crystal packing of molecules *A*, *B* and *C* in compound **1**. (*a*) View slightly off-set from the *a* axis, showing the near linear (θ = 167.8°) alignment of tail-to-tail C13*C*—H13*C*$\cdots$O6*C* intrastrand contacts and interdigitation interactions through interstrand donor propargylic H9*A* (green) and H9*B* (blue) atoms with acceptor dioxolanyl atoms O6*C* (red) and ether atoms O3*C* (red), respectively; measurement of very weak engagement between interstrand donor proparygyl H9*C* (red) and acceptor propargylic ether atoms O2*A* (green) is not shown here, but discussed in Section 3.2.3. (*b*) View along the *c* axis showing the parallel, unidirectional and tail-to-tail arrangements of strands of outstretched molecules *A* (green) and *B* (blue), and the orthogonal tail-to-tail arrangement of strands of molecules *C* (red), all with acetylenic donor C13—H13$\cdots$O6 dioxolanyl acceptor contacts; the positions of atoms C5 and H9 are also shown for reference purposes. Generic atom labels without symmetry codes have been used.

Table 2
Selected torsion data for the alignment of head and tail dioxolanyl and propargyloxy groups, with each other and independently relative to the central mannitol chain of each of the crystallographically independent molecules *A*–*C* in the unit cell of compound **1**, showing individual torsion angles (φ), mean values within each head and tail group, and observed deviations from the means[a].

Entry	Position	Torsions	Angle, φ (°)	*A*–*C* Mean, φ (°) (±deviation)
1	central	C3*A*—C6*A*—C10*A*—C16*A*	−176.7 (2)	180.0 (2.3)[b]
2	central	C3*B*—C6*B*—C10*B*—C16*B*	175.2 (2)	180.0 (−4.8)[b]
3	central	C3*C*—C6*C*—C10*C*—C16*C*	175.5 (2)	180.0 (−4.8)[b]
		C—C3/16—C6/10—C	Dioxolanyl(C)—C relative to core(C)	
4	head	C2*A*—C3*A*—C6*A*—C10*A*	76.6 (2)	78.7 (−2.1)
5	head	C2*B*—C3*B*—C6*B*—C10*B*	80.6 (2)	78.7 (1.9)
6	head	C2*C*—C3*C*—C6*C*—C10*C*	78.9 (2)	78.7 (0.2)
7	tail	C6*A*—C10*A*—C16*A*—C15*A*	85.0 (2)	77.4 (7.6)
8	tail	C6*B*—C10*B*—C16*B*—C15*B*	73.8 (2)	77.4 (−3.6)
9	tail	C6*C*—C10*C*—C16*C*—C15*C*	73.3 (2)	77.4 (−4.1)
		O—C3/16—C6/10—C	Dioxolanyl(O)—C relative to core(C)	
10	head	O2*A*—C3*A*—C6*A*—C10*A*	−167.1 (2)	−165.0 (−2.1)
11	head	O2*B*—C3*B*—C6*B*—C10*B*	−163.4 (2)	−165.0 (1.6)
12	head	O2*C*—C3*C*—C6*C*—C10*C*	−164.4 (2)	−165.0 (0.6)
13	tail	C6*A*—C10*A*—C16*A*—O5*A*	−159.5 (2)	−166.8 (7.3)
14	tail	C6*B*—C10*B*—C16*B*—O5*B*	−170.2 (2)	−166.8 (−3.4)
15	tail	C6*C*—C10*C*—C16*C*—O5*C*	−170.6 (2)	−166.8 (−3.8)
		C—O2/5—C3/16—C	Dioxolanyl(C)—O relative to core(C)	
16	head	C1*A*—O2*A*—C3*A*—C6*A*	−152.2 (2)	−148.2 (−4.0)
17	head	C1*B*—O2*B*—C3*B*—C6*B*	−149.9 (2)	−148.2 (−1.7)
18	head	C1*C*—O2*C*—C3*C*—C6*C*	−142.4 (2)	−148.2 (5.3)
19	tail	C14*A*—O5*A*—C16*A*—C10*A*	−137.4 (2)	−137.9 (0.5)
20	tail	C14*B*—O5*B*—C16*B*—C10*B*	−139.2 (2)	−137.9 (−1.3)
21	tail	C14*C*—O5*C*—C16*C*—C10*C*	−137.0 (2)	−137.9 (0.9)
		O—C6/10—C10/6—C	Propargyl(O) relative to core(C)	
22	head	O3*A*—C6*A*—C10*A*—C16*A*	−52.4 (2)	−58.2 (5.8)
23	head	O3*B*—C6*B*—C10*B*—C16*B*	−61.4 (2)	−58.2 (−3.2)
24	head	O3*C*—C6*C*—C10*C*—C16*C*	−60.8 (2)	−58.2 (−2.6)
25	tail	C3*A*—C6*A*—C10*A*—O4*A*	−54.4 (2)	−58.7 (4.3)
26	tail	C3*B*—C6*B*—C10*B*—O4*B*	−61.0 (2)	−58.7 (−2.3)
27	tail	C3*C*—C6*C*—C10*C*—O4*C*	−60.7 (2)	−58.7 (−2.0)
		C—O3/4—C6/10—C	Propargyl(C)—O relative to core(C)	
28	head	C7*A*—O3*A*—C6*A*—C10*A*	148.0 (2)	148.1 (−0.1)
29	head	C7*B*—O3*B*—C6*B*—C10*B*	149.0 (2)	148.1 (0.9)
30	head	C7*C*—O3*C*—C6*C*—C10*C*	147.4 (2)	148.1 (−0.7)
31	tail	C11*A*—O4*A*—C10*A*—C6*A*	142.6 (2)	140.3 (2.3)
32	tail	C11*B*—O4*B*—C10*B*—C6*B*	138.2 (2)	140.3 (−2.1)
33	tail	C11*C*—O4*C*—C10*C*—C6*C*	140.1 (2)	140.3 (−0.2)
		C—O3/4—C7/11—C	Propargyl(C)—C relative to core(C)	
34	head	C6*A*—O3*A*—C7*A*—C8*A*	−58.5 (2)	−68.9 (10.4)
35	head	C6*B*—O3*B*—C7*B*—C8*B*	−72.9 (2)	−68.9 (−4.0)
36	head	C6*C*—O3*C*—C7*C*—C8*C*	−75.3 (2)	−68.9 (−6.4)
37	tail	C10*A*—O4*A*—C11*A*—C12*A*	−86.2 (2)	−79.4 (−6.8)
38	tail	C10*B*—O4*B*—C11*B*—C12*B*	−63.2 (2)	−79.4 (15.2)
39	tail	C10*C*—O4*C*—C11*C*—C12*C*	−88.7 (2)	−79.4 (−9.3)

Notes: (*a*) the colours highlight the torsions of most difference within each triplet: red 2–7°, green 7–12° and blue >12°. (*b*) Deviation from the ideal angle of 180°.

has been reported (Mohammed *et al.*, 2012) and the X-ray diffraction sample crystallized from EtOAc/*n*-hexane as colourless prisms (m.p. 50–52 °C).

2.2. Refinement

Crystal data, data collection and structure refinement details are summarized in Table 1. The H atoms were not located in the difference Fourier map. Instead, the H atoms were placed geometrically and constrained according to their environment.

2.3. Analyses of the Cambridge Structural Database (CSD)

2.3.1. Searches of the CSD based on *Mercury* Crystal Packing Features (PFF). A total of 33 individual searches of the Cambridge Structural Database (CSD; Groom *et al.*, 2016) for Crystal Packing Features (referred to here as PFFs) and illustrated in Fig. S1 (see supporting information) were carried out on 11 unique sets of donor *D* (A1, A2, B, C and D) and acceptor *A* (E, F, G, H, I and J) propargylic contacts that were recognised within the crystal structure of compound **1** (Fig. S2). Search criteria specified consideration of 'Cyclicity'

Table 3
Short intrastrand and interstrand contacts between like molecules from each of strands *A*–*C*.

Strand/ Entry	Intra/ inter strand	*D*···*A* positions	*D*—H···*A*	*D*—H	H···*A*	*D*···*A*	Contact angle, θ
A							
1	intra	tail–tail	C13*A*—H13*A*···O6*A*^{i}	0.95	2.34	3.247 (3)	158.3
2	inter	head–tail	C5*A*—H5*A*A···C13*A*^{ii}	0.98	3.39	3.466 (4)	86.1
3	inter	tail–head	C17*A*—H17*B*···C8*A*^{ii}	0.98	2.98	3.652 (3)	127.1
B							
4	intra	tail–tail	C13*B*—H13*B*···O6*B*^{i}	0.95	2.21	3.138 (2)	164.7
5	intra	tail–tail	C13*B*—H13*B*···C14*B*^{i}	0.95	2.98	3.884 (3)	159.5
6	intra	tail–tail	C13*B*—H13*B*···C17*B*^{i}	0.95	3.04	3.827 (4)	141.2
7	intra	tail–tail	C17*B*—H17*D*···H13*B*^{i}	0.98	2.57	3.04	109.5
8	inter	head–tail	C5*B*—H5*BB*···C12*B*^{ii}	0.98	3.10	3.612 (3)	114.4
9	inter	tail–head	C17*B*—H17*E*···C7*B*^{ii}	0.98	3.09	3.919 (4)	143.0
10	inter	tail–head	C17*B*—H17*E*···C8*B*^{ii}	0.98	3.06	3.812 (4)	134.1
11	inter	tail–head	C18*B*—H18*E*···C9*B*^{ii}	0.98	3.05	3.861 (5)	141.1
C							
12	intra	tail–tail	C13*C*—H13*C*···O6*C*^{ii}	0.95	2.34	3.278 (3)	167.8
13	intra	head–head	C4*C*—H4*CB*···C9*C*^{ii}	0.98	3.02	3.456 (4)	108.3
14	inter	head–tail	C4*C*—H4*CC*···C18*C*^{iii}	0.98	2.92	3.867 (4)	162.5

Symmetry codes: (i) $x-1, y, z$; (ii) $x, y-1, z$; (iii) $x-1, y+1, z$.

and were given a 'Low' setting tolerance 'Level of Geometric Similarity'. Where bifurcation was evident, individual PFF searches were performed for each partner pair and then for the two interactions together. The output of each search was recorded with a Positive result (a numerical and itemized list of known structures, with structure codes, that fell within the Low Level of Geometric Similarity), and a Negative result (included a corresponding numerical and itemized list of known structures containing the components of the search query, but where the geometric tolerances were not met). The reference codes of structures regarded as Positive and Negative hits under each PFF search result, and their total numbers and percentages, were compiled into *Microsoft Excel* spreadsheets. A spreadsheet of the results with matching Positive and Negative structure codes aligned (with the exception of search B1.2) was constructed (Table S2), and the numerical data summarized in graphical form (see Section 3.4.2).

2.3.2. Searches based on liberally defined structural motifs using the *ConQuest* search tool. Loosely constrained structural motifs derived from those shown in Fig. S2 were established in the *ConQuest* search tool for propargylic donor interactions: CSM_A1, CSM_A2, CSM1_R1, CSM1-R2, CSM1_R3 and CSM1_R4; and acceptor interactions: CSM1_R5 and CSM1_R6 (Fig. S3). Relevant distance parameters, D1 (H···*A*, Å) and D2 (*D*···*A*, Å), were liberally defined as within the sum of the van der Waals radii plus 1.0 Å, and the angular measurements, ANG (*D*—H···*A*, °), limited to within 60–180°. Where multiple contacts were recorded for a single compound, sometimes within the same category, these were included for

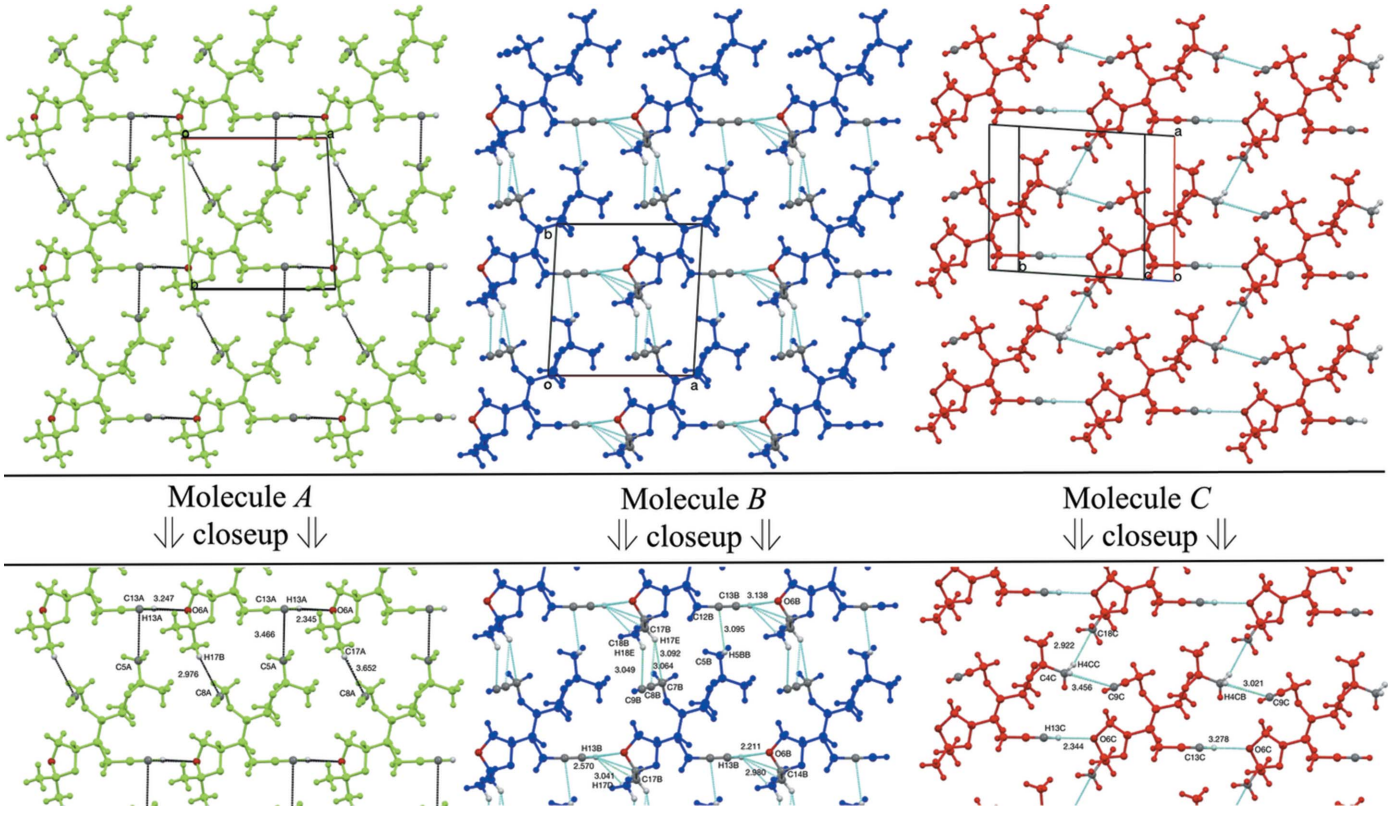

Figure 3
Inter- and intrastrand contacts between like molecules of strands *A*, *B* and *C*, as seen from directly above the mean planes of the *A*, *B* and *C* sheets, with unit cells indicated, as well as closeup views with labels and distance measurements included.

completeness. The values for D1, D2 and ANG for all matching contacts found in the CSD were recorded and the results displayed as scatterplots against 'Identity Number' in Fig. S3 and discussed more fully in Section 3.4.3.

3. Results and discussion

3.1. Molecules in the unit cell

The asymmetric unit comprises three independent molecules (represented as *A*-green, *B*-blue and *C*-red), each with the mannitol 2*R*,3*R*,4*R*,5*R* configuration [Fig. 1(*b*), randomly selected molecule *A*] and differing only in the conformation of the molecule. This establishes asymmetry in each molecule. Hence, in future, and for ease of reference, the terms 'head' and 'tail' sections will be used for each molecule, based on lower and higher crystallographic element numbers, respectively [Fig. 1(*c*)].

3.1.1. Conformations of molecules *A*–*C*. Based on torsion angles (Table 2), there are marginal differences in the conformation about the central mannitol core (Entries 1–3), with molecule *A* the most notable. Marginal differences are also observed in torsions associated with the orientation of the dioxolanyl groups relative to the core (Table 2, Entries 4–15), but most notably in molecule *A* and to the largest extent in the tail portion of the molecules. In contrast, puckering of the dioxolanyl group, as reflected in the C1/14—O3/10—C3/16—C6/10 torsion angles (Table 2, Entries 16–21), was most varied in the head section, and to the most significant extent (moderately) in molecule *C*; configurations in the tails of molecules *A*–*C* were highly consistent. The propargyloxy substituents potentially have three sources of conformational freedom. Marginal differences are observed in the torsions associated with their attachment to the mannitol core in both head and tail sections (Table 2, Entries 22–27), but most noticeably in molecule *A*. From this point, the orientation of the propargyl groups in comparison with the mannitol core are relatively conserved in the heads and tails of all three molecules (Table 2, Entries 28–33). However, significant differences are then observed in the orientations of the terminal acetylenic groups in the head and tail sections relative to the mannitol fragment (Table 2, Entries 34–39), with the most extreme difference appearing through atom O3 in the head of molecule *A* and atom O4 in the tail of molecule *B*.

3.2. Strand and sheet assemblies

3.2.1. Recognition of the like molecular strand construct. More detailed analysis reveals that, in the crystal, the three independent species (*A*-green, *B*-blue and *C*-red) align in strands, each with matching identical molecules *A*, *B* and *C*. Molecules in each strand engage through unique tail-to-tail

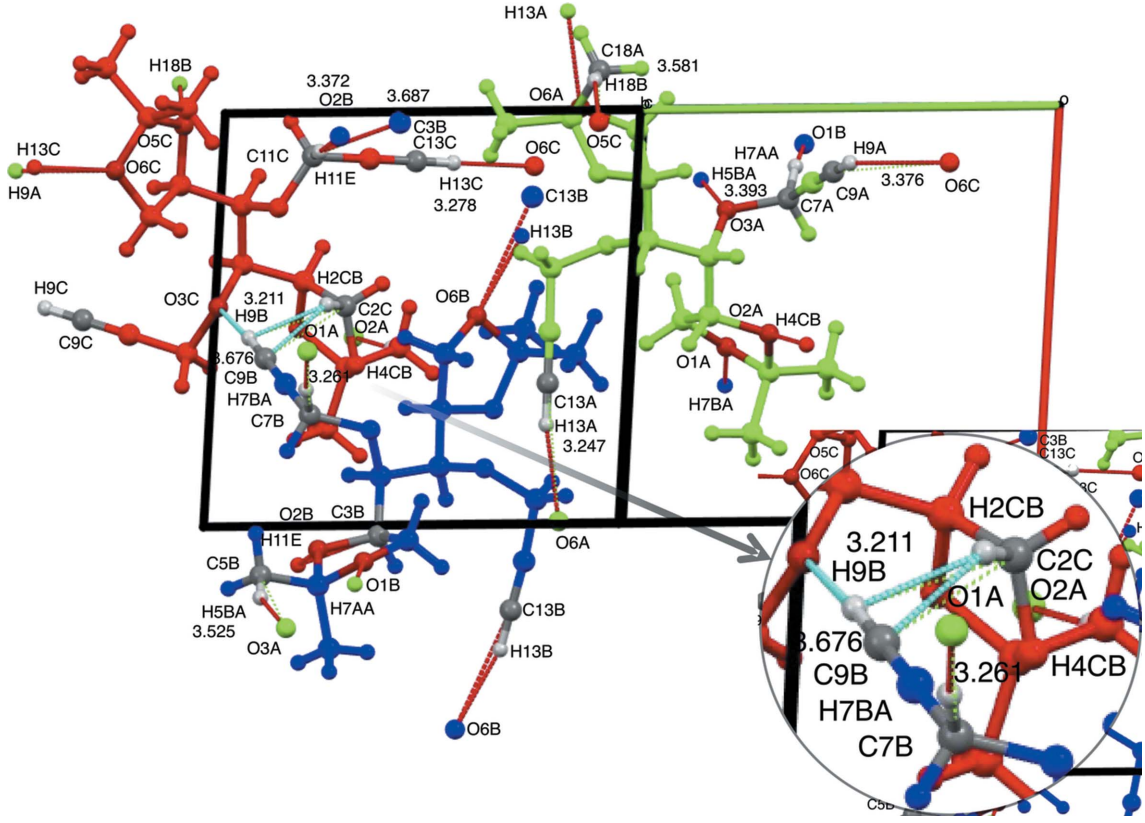

Figure 4
The unit cell of compound **1** viewed down the crystallographic *b* axis after rotating by 135° about the vertical axis, showing molecules *A* (green), *B* (blue) and *C* (red) with selected atom labels of close contacts as defined automatically within the limits of van der Waals radius −0.05 to 0.30 Å, within the crystal lattice, and an enlarged inset with details of the linear and orthogonal contacts involving C9*B*—H9*B* and C2*C*—H2*CB* with additional enforced distance measurements to C2*C* indicated. Note that the C9*C*—H9*C*···O2*A* contact was not detected under the conditions set for close contacts.

interactions. The differences in each case appear to arise because of subtle differences in the conformations of each molecule. Such individual strands all occur through C13—H13···O6 contacts and are represented and viewed along the *a* axis in Fig. 2(*a*) and along the *c* axis in Fig. 2(*b*). Thus, the contacts for molecules *A* (green) and *B* (blue) occur in a unidirectional sense along the *b* axis, with identical symmetry codes, namely $(x + 1, y, z)$, while strands of molecules *C* (red) are oriented perpendicular, along the *a* axis [consider Figs. 2(*a*) and 2(*b*)], through a different symmetry code, $(x, y - 1, z)$. As is also evident, particularly in Fig. 2(*b*) and the positions of atoms C5 and C9, the molecules in strands *A* and *B* are flipped relative to each other by approximately 180° about the length of the two strands. This feature permits near coincidence of the C13—H13···O6 alignments, with unidirectionality of the overall strands, while accommodating the steric demands of the remaining portions of the molecules.

3.2.2. Homogeneous molecular strands and sheets. *3.2.2.1. Intrastrand contacts between like molecules.* Significant advances have been made towards estimating the H-atom positions of small organic molecules from X-ray crystallographic data (Jayatilaka & Dittrich, 2008; Capelli *et al.*, 2014; Woińska *et al.*, 2016). These have achieved results that are within the accuracy of neutron diffraction. However, a very limited number of examples have been described. As a consequence, contact data for short intra- and interstrand interactions between like molecules of each type have been summarized in Table 3 using parameters that have become accepted more widely as good indicators of strength and efficiency in the field for weak hydrogen bonds (Desiraju, 2005). The values include the accurately measured *D*···*A* distance (D, Å), the estimated *D*—H bond length using the previously utilized predicted position of the H atom for each type of weak acid species [CH (acetylenic) = 0.95 Å, CH (methine at sp^3 carbon) = 1.00 Å, CH_2 (methylene) = 0.99 Å and CH_3 (methyl) = 0.98 Å], without any additional normalization, and the resulting H···*A* distance (Å). Common to each of the strands are the aforementioned intrastrand tail-to-tail C13—H13···O6 contacts (Table 3; Entries 1, 4 and 12). All three achieve short *D*···*A* distances with near-linear *D*—H···*A* contact angles (*A* 158.3, *B* 164.7 and *C* 167.8°). Observed values are consistent with acetylenic groups with pK_a (Me_2SO) ∼ 24.9 (Pedireddi & Desiraju, 1992). These intrastrand associations stand alone for molecule *A*, but are reinforced within the strands from molecule *B* by additional more distant C13—H13*B*···C14*B*, C13—H13*B*···C17*B* and C17*B*—H17*D*···H13*B* contacts (Table 3, Entries 5–7), and within those from molecule *C* by an equally distant head-to-head C4*C*—H4*CB*···C9*C* contact (Table 3, Entry 13) (see also Fig. 3). Those involving molecule *B* are exceptionally weak, as assessed by *D*···*A* distance measurements. They stem from additional engagement by the C13*B*—H13*B* group as a donor in a trifurcated contact with quaternary atom C14*B* and its neighbouring bonded methyl C17*B* and H17*D* atoms. The additional intrastrand contact involving molecules *C* is remarkable because it occurs between highly remote groups that ordinarily are weak donors and acceptors.

3.2.2.2. Interstrand contacts between like molecules. Interstrand contacts are also observed between like molecular strands (Table 3 and Fig. 3). These vary between parallel strands of molecules *A*, *B* and *C* with interstrand spacings, as measured by C13···C13′ distances of 10.300 (5), 10.300 (5) and 9.473 (4) Å, respectively, to create planar sheets of singular molecular type (Fig. 3). Donors in each case comprise normally weak dioxolanyl methyl groups, in which those between strands of *A* and *B* resemble each other, and those between strands *C* engage differently. For example, those from molecule *A* include a noticeably moderate C5*A*···C13*A* contact [*D*···*A* = 3.466 (4) Å] (Table 3, Entry 2) orthogonal to the aforementioned C13*A*—H13*A*···O6*A* interaction, while those from molecule *B* include a similar but specific C5*B*—H5*BB*···C12*B* contact [*D*···*A* = 3.612 (3) Å] (Table 3, Entry 8), neither of which are observed between the strands of molecule *C*. Similarly, molecule *A* participates in a weaker C17*A*—H17*B*···C8*A* contact with a propargylic acceptor (Table 3, Entry 3), while the equivalent donor group in molecule *B*, namely, C17*B*—H17*E*, engages in a bifurcated hydrogen-donor arrangement with the propargylic C7*B*—C8*B* bond (Table 3, Entries 9 and 10), neither of which are evident in the strands of molecule *C*. Molecule *B* is also involved in a separate propargylic H18*E*···C9*B* interaction (Table 3, Entry 11), which is absent in the strands of *A*, but is observed indirectly in those of molecule *C* (Fig. 3). Thus, molecule *C* shows a weak interstrand donor C4*C*—H4*CC*···C18*C* contact [*D*···*A* = 3.867 (4) Å], as well as the medium-strength intrastrand C4*C*—H4*CB*···C9*C* contact [*D*···*A* = 3.456 (4) Å] (Table 3, Entries 14 and 13, respectively).

A consequence of these analyses is that, despite the orthogonal alignment of strands of molecules *C* relative to those of molecules *A* and *B*, the two-dimensional array of short contacts between like molecules in compound **1** is found to result in the formation of homogenous sheets of each molecular type.

3.2.3. Cross-strand/cross-sheet interactions. Separate molecular interactions occur between, rather than within, the sheets of molecules *A*–*C*. The nonconforming orientation of the *C* strand compared with the *A* and *B* strands, in particular, led us to examine even more closely this aspect of the supramolecular structure. In addition, the intermolecular interactions involving the propargylic C9—H9 acetylene donor functional groups in the head moieties were of interest. Contact data for these cross-strand/cross-sheet contacts (contacts between donors and acceptors from different molecular types *A*–*C*), almost all of which are ostensibly stronger C—H···O contacts, are summarized in Table 4. Contact angle (θ, °), as well as distance measurements, are given for added depth of analyses. Values for intrastrand acetylenic C13—H13···O6 contacts are included for comparison (Table 4, Entries 1–3). As with the earlier analyses, it is acknowledged that the resulting data are derived from a single-crystal X-ray crystallographic study and not a comprehensive crystallographic database search. However, the observations and conclusions drawn from them are based on comparisons from well debated past literature.

Table 4
Short-contact donor (*D*) acetylenic (Entries 1–8) and non-acetylenic (Entries 9–18) H···acceptor (*A*) interactions, initially defined automatically within the limits of van der Waals radius −0.05 to 0.30 Å, and measured in Angstroms (Å), for molecules *A*–*C* in the crystal lattice of compound **1**, as well as *D*—H···*A* contact angles (θ, °), where *A* = oxygen (O) in most cases, and relevant carbon (C) and hydrogen (H) close contacts in other cases, with relevant head and tail denominations for participating groups, useful for indicating the nature of their alignment.

Entry	*D*···*A* positions	*D*—H···*A*	*D*—H	H···*A*	*D*···*A*	Contact angle, θ
1	tail–tail*	C13*A*—H13*A*···O6*A*^{i}	0.95	2.34	3.247 (3)	158.3
2	tail–tail*	C13*B*—H13*B*···O6*B*^{i}	0.95	2.21	3.138 (2)	164.7
3	tail–tail*	C13*C*—H13*C*···O6*C*^{ii}	0.95	2.34	3.278 (3)	167.8
4	head–tail	C9*A*—H9*A*···O6*C*^{iii}	0.95	2.58	3.376 (4)	140.8
5	head–head	C9*B*—H9*B*···O3*C*	0.95	2.19	3.122 (3)	167.1
6	head–head[a]	[C9*C*—H9*C*···O2*A*^{iv}	0.95	2.71	3.541 (3)	146.6]
7	head–head	C9*B*—H9*B*···C2*C*	0.95	3.21[b]	3.676 (3)	112.1
8	head–head	C9*B*—H9*B*···H2*C*B	0.95	2.35	2.78	107.4
9	head–head[b]	C2*C*—H2*CB*···C9*B*	0.99	2.78	3.676 (3)	145.4
10	head–head[b]	C2*C*—H2*CB*···H9*B*	0.99	2.35	3.21[c]	150.3
11	head–head	C7*A*—H7*AA*···O1*B*^{v}	0.99	2.55	3.393 (2)	142.5
12	head–head	C7*B*—H7*BA*···O1*A*^{ii}	0.99	2.29	3.261 (2)	165.8
13	tail–head	C11*C*—H11*E*···O2*B*^{vi}	0.99	2.38	3.372 (3)	176.9
14	tail–head	C11*C*—H11*E*···C3*B*^{vi}	0.99	2.82	3.687 (4)	146.7
15	head–tail	C6*C*—H6*C*···O5*A*^{vii}	1.00	2.67	3.457 (2)	135.6
16	tail–head	C16*B*—H16*B*···O1*C*	1.00	2.69	3.584 (3)	149.1
17	head–head	C4*C*—H4*CB*···O2*A*^{vii}	0.98	2.57	3.535 (3)	169.1
18	head–head	C5*B*—H5*BA*···O3*A*^{v}	0.98	2.59	3.525 (3)	160.0
19	tail–tail	C18*A*—H18*B*···O5*C*^{v}	0.98	2.62	3.581 (3)	168.1

Symmetry codes: (i) $x-1, y, z$; (ii) $x, y-1, z$; (iii) $x, y-1, z-1$; (iv) $x, y+1, z+1$; (v) $x-1, y-1, z$; (vi) $x+1, y, z$; (vii) $x, y, z-1$. Notes: (*a*) Not visible in Fig. 4. (*b*) Non-acetylenic donor (*D*) and acetylenic acceptor (*A*) (see Fig. 6). (*c*) The C2*C*···H9*B* contact distance falls outside the constraints set for others and the value was obtained by targeted measurement. (*) Denotes an intrastrand interaction.

Cross-strand acetylenic C9—H9 donor interactions occur from molecules *A*, *B* and *C* (Table 4, Entries 4–6). Superficially, those from molecules *A* (green) and *B* (blue) engage in unique finger-like intrusions, that are almost perpendicular to the axis of the parent strand, into separate strands of molecules *C* (red) [Fig. 2(*b*)], yet each one of the three contacts is different in detail. Readers will find Fig. 4 helpful in providing a pictorial view of the short contacts within the unit cell, as expressed in Table 4.

3.2.3.1. Cross-strand interactions from the standpoint of donor elements. Interstrand interactions are grouped in Table 4 according to notional donor acid strength, as defined by calculated *D*—H bond lengths, which are based on donor-atom electronegativity. This classification does not correlate directly with the understood mark of contact strength, namely, *D*···*A* distance, even when contact angle (θ) is considered. The interactions in Table 4 are therefore discussed in this order, but within the context of three interaction types: *singlet*, *pivot* and *couplet* (see Fig. 5).

Molecules *A* (green) provide a modest cross-strand C9*A*—H9*A* acetylenic donor interaction with the tail dioxolanyl O6*C* atom in addition to the strong intrastrand, C13*C*—H13*C* donor contact with the same acceptor (Table 4, Entries 3 and 4). Because the acceptor O6*C* serves as a fulcrum in bringing together adjacent *A* and *C* molecules, the contact is called here a '*pivot*' interaction [Fig. 5(*a*)]. The short-to-medium C9*A*—H9*A*···O6*C* contact distance [D = 3.376 (4) Å] is consistent with a slightly weaker acid than the acetylenic C13—H13 groups (Pedireddi & Desiraju, 1992). Its contact angle (140.8°) (Table 4, Entry 4) is far from the near linear alignment of its partner (167.8°; Table 4, Entry 3) but within the range of other contacts from weak acids where interactions have been attributed to electrostatics (Desiraju, 1990; Pedireddi & Desiraju, 1992). However, in this pivot case, where both donors are of the same chemical type, the different *D*···*A* distances is most likely a reflection of the different contact angles, with the linear contact being more dominant.

In a separate pivot interaction [Fig. 5(*e*)], molecules *C* (red) demonstrate a somewhat longer [D = 3.541 (2) Å] acetylenic donor contact (C9*C*—H9*C*···O2*A*; Table 4, Entry 6), identified only by a directed measurement (therefore not visible in Fig. 4) with the head dioxolanyl group of an *A* molecule. The interaction is associated with another nonlinear contact angle (146.6°), but in this case made with a near linear contact (169.1°) with its pivot donor partner C4*C*—H4*C*B (Table 4, Entry 17). The donor in this portion of the pivot is derived from a dioxolanyl methyl group, which would normally be a much less acidic proton source than a terminal acetylene group (compare the estimated *D*—H bond lengths of 0.98 *versus* 0.95 Å). The observed *D*···*A* distances for the two interactions are indicative of the anticipated donor strengths, but closer in magnitude than one might expect. One explanation for their similarity is the acute angle of the first, which would diminish the donor effectiveness from pK_a, and linearity of the latter, which would enhance effectiveness from pK_a for the methyl H atoms that are already the most acidic of those attached to sp^3 C atoms in compound **1**.

Contrasting these dioxolanyl contacts, molecules *B* (blue) participate in extremely short donor acetylenic C9*B*—H9*B* interactions [D = 3.121 (3) Å] with the head O3*C* propargylic ether O atom of molecules *C* (red) (see Fig. 4 and enlargement), with an accordingly near-linear contact angle (167.1°) (Table 4, Entry 5). The acetylenic C9*B*—H9*B* bond is also engaged in a secondary near-orthogonal contact with the nearby C2*C*—H2*C* bond (Fig. 4). This geometry is supported by the H9*B*—C9*B*···C2*C*—H2*CB* torsion angle (φ = 83.8°; not recorded in Table 2) and small contact angles associated when the *D*—H group is considered C9*B*—H9*B* (107.4 and 112.1°; Table 4, Entries 7–8). However, the widely differing contact distance measurements (Table 4, Entries 7–10) for H···*A* (D = 2.35–2.78 Å) and *D*···*A* [D = 2.78–3.676 (3) Å] reflect a highly distorted orthogonal cluster. The closer contact between participants H2*CB*···C9*B* (2.78 Å) than H9*B*···C2*C* (3.21 Å) and larger contact angle values with C2*C*—H2*CB* as the *D*—H group (145.5 and 150.3°) (Table 4, Entries 9–10) are most consistent with C2*C*—H2*CB*···C9*B* being the main contact. This secondary interaction is suggestive of a bifurcated H2*CB* (Desiraju, 1991), which probably contributes to the extreme shortness of the C9*B*···O3*C* distance.

These contacts, together, contribute to another type of co-operative set of contacts, called here a '*couplet*', that include in this example the non-acetylenic dioxolanyl methine C16*B*—H16*B*···O1*C* contact [Table 4, Entry 16; Fig. 5(*d*)]. This is one of three couplet interactions [Figs. 5(*b*)–(*d*)] observed in the

crystals of compound **1** that, by definition, bring together two interstrand partners through two independent $D\cdots A$ contacts. In this example, the bifurcated H-atom donor from C2*C*—H2*CB* and its contact with the acetylenic C9*B* as an acceptor contribute to a 'symmetrical' (donor and acceptor in each molecular contributor) 11-membered ring of couplet atoms. Alternatively, the bifurcated H atom can be considered as contributing to a wider 15-membered 'unsymmetrical' couplet involving the C9*B*—H9*B*$\cdots$O3*C* contact; in this situation, the two donor components participate from *B* molecules while the acceptors are located in *C* molecules in an unsymmetrical alliance. Couplets of either type can limit conformational flexibility and distort normal contact angles or, through their attractive nature, force contacts closer together. In the case of the methine C16*B*—H16*B*$\cdots$O1*C* interaction, the $D\cdots A$ contact distance [D = 3.584 (3) Å] (Table 4, Entry 16) is

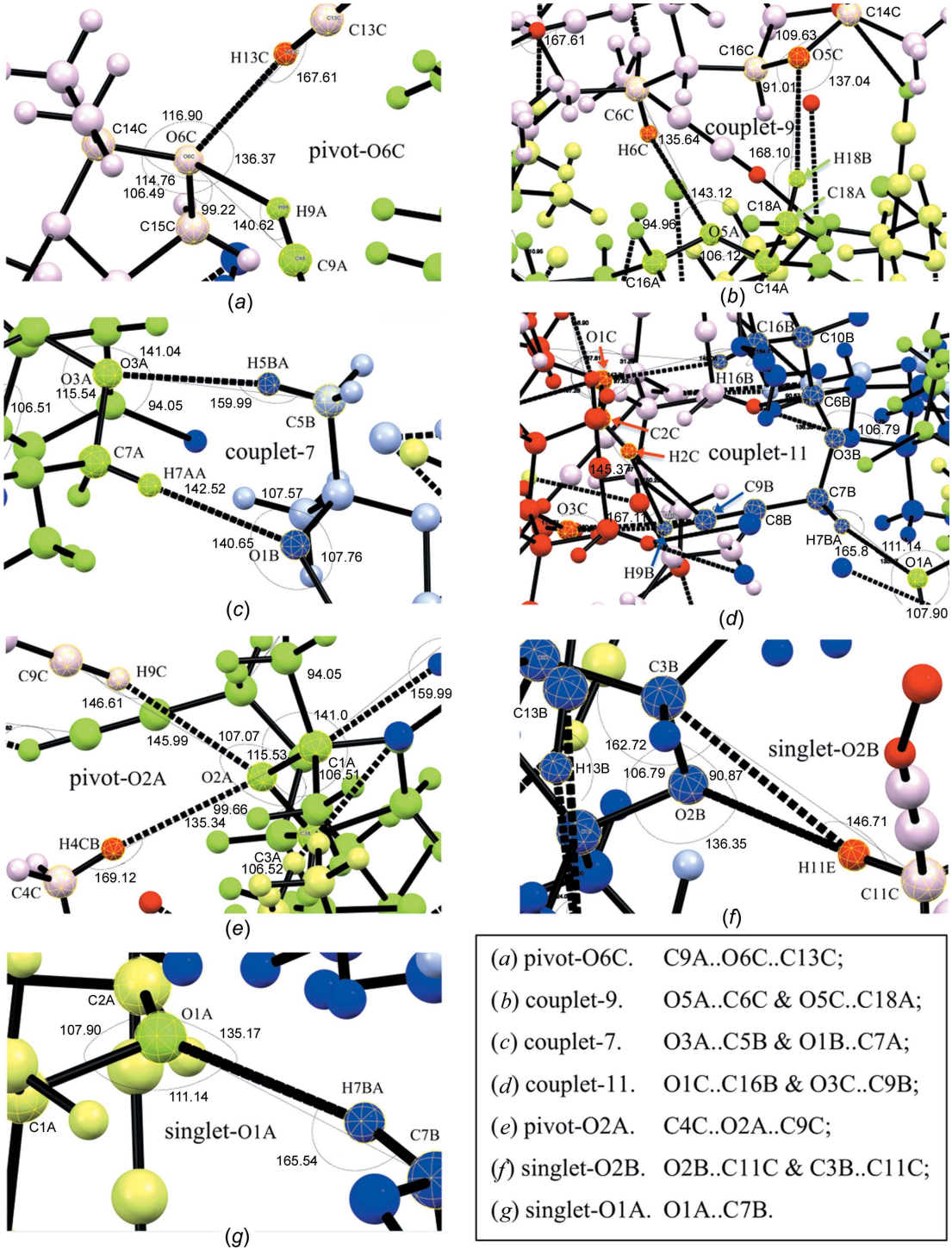

(*a*) pivot-O6C.	C9A..O6C..C13C;
(*b*) couplet-9.	O5A..C6C & O5C..C18A;
(*c*) couplet-7.	O3A..C5B & O1B..C7A;
(*d*) couplet-11.	O1C..C16B & O3C..C9B;
(*e*) pivot-O2A.	C4C..O2A..C9C;
(*f*) singlet-O2B.	O2B..C11C & C3B..C11C;
(*g*) singlet-O1A.	O1A..C7B.

Figure 5
Major types of oxygen-acceptor-centred short interstrand contacts in the X-ray crystal structure of compound **1**, with key atomic labels and bond angles, as recorded by *Mercury* (Version 2020.3.0; Macrae *et al.*, 2020), for molecules *A* (green), *B* (blue) and *C* (red).

somewhat longer than for the only other methine contact, C6*C*—H6*C*···O5*A* (Entry 15), for which the contact angle is smaller. However, it is nearly identical to those of the pivot partners around O2*A* (Table 4, Entries 6 and 17), wherein contact angles are unequal. It is also very similar to those of methyl donor contacts C5*B*—H5*B*···O3*A* and C18*A*—H18*B*···O5*C* (Entries 18 and 19) with more linear contact angles. The medium-to-large *D*···*A* distance in the case of C16*B*—H16*B*···O1*C* is possibly the result of it being part of a reasonably large couplet of atoms, and its contact angle the result of confinement of the donor C16*B*—H16*B* bond as part of the tail dioxolanyl ring system in molecule *B*.

Three non-acetylenic donor types of C—H···O close contacts are recognisable within the distance range initially defined, and all are cross-strand (see Fig. 3). Those recorded as Entries 11–14 in Table 4 are considered in the first category because they involve similarly weakly acidic *D*—H participants (note the longer estimated *D*—H distances for Entries 9–14 compared with those for the acetylenic donor examples in Entries 1–8). They proceed from the methylene groups at atoms *C*7 and C11 in the head and tail propargyloxy substituents, respectively, but their interactions are in turn each different.

Molecules *A* and *B* make reciprocal head-group methylene contacts with the dioxolanyl O1 acceptor from the partner molecule. Notably, the donor from molecule *B* (Entry 12) makes a '*singlet*' contact with O1*A* [Fig. 5(*g*)], that is, a contact without the involvement of any other partner. The singlet C7*B*—H7*BA*···O1*B* contact is closer [D = 3.261 (2) Å] and more linear (165.8°) than the C7*A*—H7*AA*···O1*B* contact from molecule *A* [Entry 11; D = 3.393 (2) Å, θ = 142.5°], which is part of another symmetrical seven-membered couplet [Fig. 5(*c*)] with the donor methyl C5*B*—H5*BA*···O3*A* interaction [Entry 18, D = 3.525 (3) Å, θ = 160.0°]. The smaller ring size of this tight couplet appears to impart a more acute angle to the C7*A*—H7*AA*···O1*B* contact and thereby must reduce the *D*···*A* distance. In contrast, only C11*C*—H11*E* participates as donor from the equivalent methylene group of molecule *C*, but the same donor makes contact with two quite different acceptors, namely, dioxolanyl O2*B* and C3*B*, with very different *D*···*A* distances. However, these acceptors reside at adjacent positions in the same molecule *B* (Table 3, Entries 13 and 14), and largely for this reason the contact is defined here as a '*singlet*' interaction [Fig. 5(*f*)]. As expected, because the acceptor O2*B* has two frontier orbitals, each with lone pairs of electrons, contact with O2*B* is much shorter and more linear [Entry 13, D = 3.372 (3) Å, θ = 176.9°] with respect to the predicted C11*C*—H11*E* bond than it is with the adjacent methine C3*B* acceptor [Entry 14, D = 3.687 (4) Å, θ = 146.7°], with no free bonding electron pairs. The fact that atom H11*E* is bifurcated probably accounts for the slightly longer C11*C*···O2*B* contact compared with the C7*B*···O1*A* contact, but with a distance that is tempered by the near perfect alignment of the former.

The second type of non-acetylenic donor close contacts exhibit methine donor contributions from C6*C*—H6*C* and C16*B*—H16*B*, respectively (Table 4, Entries 15 and 16). Contacts occur with interstrand dioxolanyl oxygen partners, but with only moderate *D*···*A* distances (D) and contact bond angles (θ). Both C atoms are derived from the mannitol skeleton, the first bearing a propargyloxy substituent and the other an oxygen substituent that is part of the tail dioxolanyl group. It is possibly significant that none of molecules *A*–*C* exhibit close contacts involving donor C—H bonds from either of the symmetry-equivalent atoms C10 and C3, respectively, of these positions. However, it is worth recalling that C3*B* does participate in a contact with donor C11*C*—H11*E* (Table 4, Entry 14), but only as a weak acceptor, and then with limited efficiency. Donor C16*B*—H16*B* was also mentioned earlier as a close contact with O1*C* within the first couplet complex [Fig. 5(*d*)], with C9*B*—H9*B*···O3*C*. The remaining methine donor contact, C6*C*—H6*C*···O5*A* (Table 4, Entry 15), participates in an unsymmetrical nine-membered couplet with a tail–tail methyl donor contact, C18*B*—H18*B*···O5*C* [Table 4, Entry 19; Fig. 5(*b*)]. Perhaps because of its slightly different methine donor character, the C6*C*—H6*C*···O5*A* contact has a measurably shorter *D*···*A* distance [D = 3.457 (2) Å] than the C16*B*—H16*B*···O1*C* contact [D = 3.584 (3) Å] (Table 4, Entries 15 and 16). Equally, the difference in *D*···*A* contact distances might arise from the smaller contact angle for C6*C*—H6*C*···O5*A* brought about by constraints of its smaller ring couplet than those of the larger one involving C16*B*—H16*B*···O1*C*. Finally, the three remaining non-acetylenic donor contacts emanate from a C—H bond in one of the slightly more acidic, axial or equatorial geminal methyl groups attached to the dioxolanyl groups (Table 4, Entries 17–19). The three donors interact either head–head or tail–tail with a dioxolanyl O-atom acceptor and have comparable *D*···*A* distances (D) with near-linear contact angles (θ). All three contacts have been discussed above within the context of other interactions (Table 4, Entries 6, 15, and 16).

Between them, this complex array of contacts affords stability to the observed alternating layered sheets of *A* (green)–*C* (red)–*B* (blue) molecules (Fig. 6). The arrangement leaves no interdigitation of propargyl groups between layers of molecules of type *A* (green) and *B* (blue). However, there are alternative *A*···*B* reciprocal C—H···O contacts (Table 4, Entries 11–12 and 18), of which the head-to-head propargylic C7*B*—H7*B*···O1*A* contact and nonpropargylic C5*B*—H5*BA*···O3*A* contact are most important.

With this improved understanding of contacts from the perspective of C—H donors, a brief study was made of the geometry about the most important cross-strand contact acceptors in compound **1**, the relevant dioxolanyl and propargyloxy ether O atoms.

3.2.3.2. Cross-strand interactions from the standpoint of O-atom acceptors. Data derived from measurements of individual bond and contact angles associated with covalently bound O atoms and their close intermolecular donor C—H contacts are summarized in Table 5. This process was initiated on the questionable premise that acceptor interactions would take place through O-atom lone pairs of electrons (Taylor & Kennard, 1982, 1984; Steiner & Desiraju, 1998) and with the intention of providing better insight into the geometry at the acceptor sites.

The method used acknowledges that the O atoms in molecule **1** are all ethers and should have an electron-pair geometry that is approximately tetrahedral with coordinate angles of 109.5°. Accordingly, the sum of the triplet of bond and contact angles surrounding each relevant acceptor O atom has been calculated and the geometry arbitrarily assessed as 'pyramidal' (trigonal pyramidal) or 'planar', depending on whether the angle sum is less or more, respectively, than 344°, midway between the ideal for tetrahedral (328.5°) and planar (360°). In this study, close donor–acceptor ($D\cdots A$) contacts are limited to those shorter than the sum of the van der Waals radii minus 0.01 Å. Under these conditions, atoms O2*C*, O3*B*, O4*A*–O4*C* and O5*B* showed no close contacts. In Table 5, the values of the $D\cdots A$ distance (D, Å) and contact angle (θ, °) of each observed C—H···O short contact are repeated from Table 4 and the contact types from Fig. 5 are added, all for reference purposes and as an aid to interpretation.

Surprisingly, only six of the 14 contacts with O atoms can be classified as pyramidal in their geometry. While all these are associated with dioxolanyl O atoms, not all the dioxolanyl O-atom contacts can be classified in this way. As partly discussed in the context of donors, in two of the six cases, dioxolanyl atoms O6*C* (tail) and O2*A* (head) each makes pivot contacts with two C—H donors (Table 4, Entries 3/4 and 6/17, respectively). This gives the interactions a degree of complexity, but with some hope of understanding differences in the geometry at the fulcrum, which is their O atom. In the first case [Table 5, Entries 3 and 4; Fig. 5(*a*)], two of the angular components used to evaluate the pyramidal or planar geometry about O6*C* are nearly identical, but the C15*C*—O6*A*···*D* angle differs markedly, *i.e.* 135.4 (1)° when *D* = C13*C* and 99.2 (1)° when *D* = C9*A*. The rendition of these contacts in Fig. 5(*a*) gives insight into the competition by donors C13*C*—H13*C* and C9*A*—H9*A* for access to O6*C*. It also gives an understanding as to how the closer more linear contact resulting from the former might have arisen through an overall planar geometry with O6*C*, with a splaying of the C15*C*—O6*A*···C13*C* angle, and a slightly weaker more apical contact at O6*C* through an acute angular interaction (probably electrostatic) by C9*A*—H9*A*. In the second pivot example [Table 5, Entries 9 and 10; Fig. 5(*e*)], a similar interplay appears to be involved, but the less acidic donor partner, C4*C*—H4*CB*, exerts a closer than expected near-linear contact with acceptor O2*A* at an angle sum [341.5 (2)°] that is close to being defined as that for a planar contact. As a result, the C1*A*—O2*A*···C4*C* and C3*A*—O2*A*···C9*C* component angles are increased and the C9*C*—H9*C*···O2*A* contact weakened concomitantly with a decrease in the observed contact angle to 146.6°.

Analyses of observed geometries around each of the O-atom acceptors in the three sets of couplet interactions reported in Table 5 (Entries 5–8 and 13–14) reveal that the observations are consistent with similar compromises in individual contributing angular components, contact distances and contact angles, but with additional consideration of the nature and size of the couplet. For example, in the symmetrical nine-membered couplet involving O5*A* and O5*C* [Fig. 5(*b*)], the unequal length of the carbon bridge between the donor and acceptor in molecule *A* (four atoms) and molecule *C* (five atoms) causes a severe enlargement of the internal C14*A*—O5*A*···C6*C* angle [143.1 (1)°] at the expense of the C16*A*—O5*A*···C6*C* angle [95.0 (1)°]. At the same time, the connectivity of the two $D\cdots A$ systems imposes the reverse distortion of the corresponding individual angles around O5*C*, with a

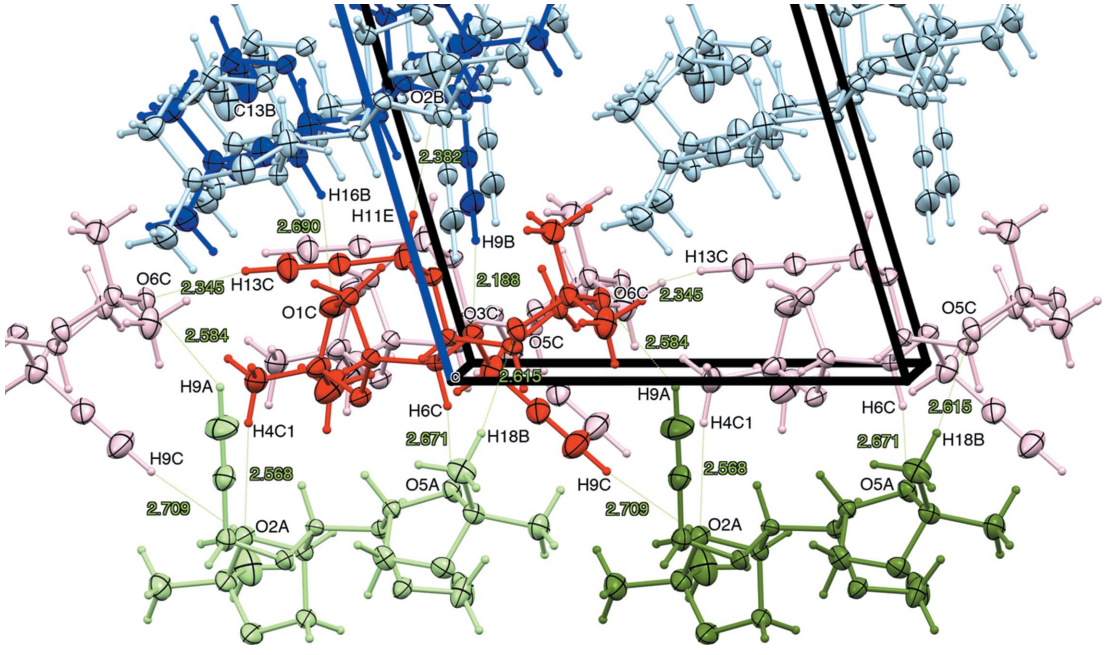

Figure 6
Close up of compound **1**, viewed along the *a* axis, with a slight offset showing differing interdigitation of C9—H9···O interactions between layers of independent molecules *A* (green), *B* (blue) and *C* (red), represented with non-H atoms as ellipsoids for clarity; key C—H donor partners are shown in darker colours.

Table 5
Analysis of the geometry of close intermolecular contacts, as defined as shorter than the sum of the van der Waals radii minus 0.01 Å, through measurement of triplet component angles at each of the key O-atom acceptor atoms[a] in molecules *A*–*C* of compound **1**, the arithmetic sum of the individual angles and resulting assignment of configuration, and duplicate records of relevant *D*···*A* distances (Å) and C—H···O contact angles, θ (°), with the contact type.

Triplet Entry	*D*···*A* positions	Component angles	Angle (°)	Angle sum (°) Configuration[b] *D*···*A* (Å)	Contact type C—H···O Angle (°)
1		C14*A*—O6*A*—C15*A*	106.41 (15)	328.9 (2)	
		C14*A*—O6*A*···C13*A*	110.9 (1)	pyramidal	singlet-O6*A*
	tail–tail	C15*A*—O6*A*···C13*A*	111.6 (1)	3.247 (3)	158.3
2		C14*B*—O6*B*—C15*B*	106.73 (14)	341.8 (2)	
		C14*B*—O6*B*···C13*B*	111.0 (1)	pyramidal	singlet-O6*B*
	tail–tail	C15*B*—O6*B*···C13*B*	124.1 (1)	3.138 (2)	164.7
3		C14*C*—O6*C*—C15*C*	106.49 (14)	358.8 (2)	
		C14*C*—O6*C*···C13*C*	116.9 (1)	planar	pivot-O6*C*
	tail–tail	C15*C*—O6*C*···C13*C*	135.4 (1)	3.278 (3)	167.8
4		C14*C*—O6*C*—C15*C*	106.49 (14)	320.5 (13)	
		C14*C*—O6*C*···C9*A*	114.8 (1)	pyramidal	pivot-O6*C*
	head–tail*	C15*C*—O6*C*···C9*A*	99.2 (1)	3.376 (4)	140.8
5		C14*A*—O5*A*—C16*A*	108.14 (1)	346.2 (1)	
		C14*A*—O5*A*···C6*C*	143.1 (1)	planar	couplet-9
	head–tail*	C16*A*—O5*A*···C6*C*	95.0 (1)	3.457 (2)	135.6
6		C14*C*—O5*C*—C16*C*	109.83 (15)	337.8 (2)	
		C14*C*—O5*C*···C18*A*	137.0 (1)	pyramidal	couplet-9
	tail–tail*	C16*C*—O5*C*···C18*A*	91.0 (1)	3.581 (3)	168.1
7		C6*A*—O3*A*—C7*A*	115.53 (14)	350.5 (1)	
		C6*A*—O3*A*···C5*B*	141.0 (1)	planar	couplet-7
	head–head*	C7*A*—O3*A*···C5*B*	94.0 (1)	3.525 (3)	160.0
8		C6*C*—O3*C*—C7*C*	114.70 (16)	352.3 (2)	
		C6*C*—O3*C*···C9*B*	131.0 (1)	planar	couplet-11
	head–head*	C7*C*—O3*C*···C9*B*	106.6 (1)	3.122 (3)	167.1
9		C1*A*—O2*A*—C3*A*	106.52 (15)	359.6 (2)	
		C1*A*—O2*A*···C9*C*	107.1 (1)	planar	pivot-O2*A*
	head–head*	C3*A*—O2*A*···C9*C*	146.0 (1)	3.541 (3)	146.6
10		C1*A*—O2*A*—C3*A*	106.52 (15)	341.5 (2)	
		C1*A*—O2*A*···C4*C*	135.3 (1)	pyramidal	pivot-O2*A*
	head–head*	C3*A*—O2*A*···C4*C*	99.7 (1)	3.535 (3)	169.1
11		C1*B*—O2*B*—C3*B*	106.77 (15)	334.1 (2)	singlet-O2*B*
		C1*B*—O2*B*···C11*C*	136.4 (1)	pyramidal	(146.7)[c]
	tail–head*	C3*B*—O2*B*···C11*C*	90.9 (1)	3.372 (3)	176.9
12		C1*A*—O1*A*—C2*A*	107.92 (17)	354.2 (2)	
		C1*A*—O1*A*···C7*B*	111.1 (1)	planar	singlet-O1*A*
	head–head*	C2*A*—O1*A*···C7*B*	135.2 (1)	3.261 (2)	165.8
13		C1*B*—O1*B*—C2*B*	107.75 (16)	356.1 (2)	
		C1*B*—O1*B*···C7*A*	107.6 (1)	planar	couplet-7
	head–head*	C2*B*—O1*B*···C7*A*	140.7 (1)	3.393 (2)	142.5
14		C1*C*—O1*C*—C2*C*	107.30 (16)	352.9 (2)	
		C1*C*—O1*C*···C16*B*	147.7 (1)	planar	couplet-11
	tail–head*	C2*C*—O1*C*···C16*B*	97.9 (1)	3.584 (3)	149.1

Notes: (*a*) atoms O2*C*, O3*B*, O4*A*–O4*C* and O5*B* showed no close contacts. (*b*) Configuration assigned arbitrarily based on the magnitude of the angle sum: pyramidal <344° and planar >344°. (*c*) The C11*C*—H11*C*···C3*B* angle.

compression of the internal C16*C*—O5*C*···C18*A* angle [91.0 (1)°] at the expense of the C14*C*—O5*C*···C18*A* angle [137.0 (1)°]. The resulting shorter *D*···*A* contact for the former [D = 3.457 (2) Å] takes place through an acute *D*—H···*A* angle (135.6°) and planar though angularly distorted interaction with O5*A*. This result occurs despite the more linear (168.1°) contact of the normally more acidic methyl donor C18*A*—H18*B* with its couplet partner O5*C*. Analysis of the seven-membered couplet [Table 5, Entries 7 and 13; Fig. 5(*c*)] provides a similarly satisfying explanation for angular distortions around the O1*B* and O3*A* acceptors and indicates a more convincing dominance of one contact, the C7*A*—H7*AA*···O1*B* interaction, over the other.

The situation in the 11-membered couplet [Table 5, Entries 8 and 14; Fig. 5(*d*)] is more complex because of the participation of the orthogonal donor arrangement of the bifurcated H2*C* atom, but it is clear that equally explicable distortions of contributing angles around key acceptor components O1*C*, C9*B* and O3*C* do take place as a result of the couplet arrangement of the two partner components. Equally, tolerated distortions around the O2*B* and O1*A* acceptor O atoms in the two singlet cases [Table 5, Entries 11 and 12; Figs. 5(*f*) and 5(*g*)] are explicable for the simple reasons of neighbouring-atom participation and crystallographic dislocation of participants.

3.3. Crystal packing

A review of the crystallographic data to this point highlights a number of noteworthy features about compound **1**. The three independent molecules *A*–*C* that make up the unit cell differ subtly in conformation, but significantly at two of their ether sites. They each assemble into unique linear strands of like molecules, primarily through C13—H13···O6 contacts, but supported by intramolecular and intrastrand interactions. Furthermore, the assemblies are unidirectional, with the strands of *A* and *B* aligned in close proximity, head-to-tail, along the crystallographic *a* axis and those of *C* aligned orthogonal along the *b* axis. Additional interstrand interactions between like molecules establish a two-dimensional sheet array of like parallel strands. However, a network of donor–acceptor contacts occur between strands/sheets of unlike molecular type.

3.3.1. Molecular strand and sheet planes. Initial examination of the crystal packing reveals a repeat layering of the three molecular types in the order *A* (green)–*B* (blue)–*C* (red), when viewed along the *a* and *b* axes (Fig. 7). Analysis of the mean planes of each molecule across three separate strands confirms their parallel arrangement, which is most convincing in Fig. 7(*a*). Such layering is consistent with the establishment of sheets (Section 3.2.2.2).

Further analysis of the mean planes of the *A*, *B* and *C* molecules in their respective strands across a span of five molecules in each strand reveals tilts of 6.28, 12.51 and 23.52°, respectively, from the mean planes of the sheets of each molecular type, which are themselves separated unequally by

$A\cdots B$ = 4.934 Å, $B\cdots C$ = 4.866 Å and $C\cdots A$ = 5.012 Å (Fig. 8).

In Fig. 7, the C13—H13-bearing propargyl group in each molecule is highlighted by encircling the group. Collectively the orientations of the encircled groups reinforce their orthogonality in the *A* and *B* strands relative to those in the *C* strands. The intrusion of the equivalent C9—H9-bearing propargyl groups from molecules *A* and *B* into the strands of molecule *C* and reciprocal angular intrusion of the group from molecule *C* only into strands of molecule *A* is noticeable in Fig. 7(*a*), and accounts for the minor differences in inter-sheet spacings. This leaves very little interaction between molecules *A* and *B*, as is evident in Fig. 7(*b*) and as was discussed in Section 3.2.3.1. Minor void spaces are visible, especially in Fig. 7(*b*), but these are too small for any molecular inclusions.

3.4. CSD searches based on *Mercury* Crystal Packing Features and *ConQuest* search motifs involving donor and acceptor acetylenic contacts observed in compound 1.

3.4.1. Background. In the preceding diffraction studies of compound **1**, intra- and intermolecular contacts were observed in which acetylenic components of the two propargyl groups participated in various situations as C—H donors and as C—H acceptors. Two principal searches of the Cambridge Structural Database (CSD; Groom *et al.*, 2016) were carried out in order to ascertain the prevalence of these interactions and their scope in crystal engineering. These comprised firstly a *Mercury*-based study using highly constrained contact motifs derived from its Crystal Packing Feature (PFF) (Fig. S1) using measurements taken directly from compound **1** (Fig. S2). The second study utilized the *ConQuest* search tool and more loosely defined motifs (CSM) (Fig. S3) that, while artificial in their construct, were again based on general interpretations of the observed contacts (Fig. S2). The outcomes of these searches are discussed separately.

3.4.2. Analysis of *Mercury* Crystal Packing Feature (PFF) search results. As a general observation from the results summarized in Fig. 9 and Table S2, the propargylic group gave more positive matches when it participated as a donor through its terminal acetylenic proton than when the group served as a proton acceptor (Fig. 9). An analysis of findings from each contact type is described in detail in the supporting information, and summarized in the following sections.

3.4.2.1. Propargyl group as donor. There were considerable differences when the propargyl group served as a donor. Searches C and D were the more populous in terms of positive and negative results, while search B was extremely variable, especially with respect to negative results. Searches were dependent upon $D\cdots A$ distances, with the observed shorter distances of stand-alone strand-forming contacts in group A being less common than equivalent interstrand contact distances or distances involving shared contacts with adjacent acceptor atoms. This dependence showed strong variation with the nature of the acceptor atom and with the number and extent of prescription, including Cyclicity, in the atoms/groups associated with the acceptor atom.

3.4.2.2. Propargyl group as acceptor. Despite many fewer positive results from motifs E–J than from motifs A–D, the number of negative results from searches remained in excess of 70 in cases E–I3, and there was less scope than in the A–D cases for varying attached groups to either *D* or *A* atoms. Cases G1.1 and H1.1 provided situations with equivalent *D* and *A* types where minor differences in numbers of positive results (1 *versus* 3, respectively, perfectly counterbalanced by the differences in negative results, 75 *versus* 73) were observed. It was not possible to determine if these resulted intrinsically from very slightly higher $D\cdots A$ contact distances, or ultimately by the significantly different D—H$\cdots A$ bond angles brought about by intermolecular intrastrand (G1.1) compared with interstrand (H1.1) contacts (Fig. 3 and Table 4).

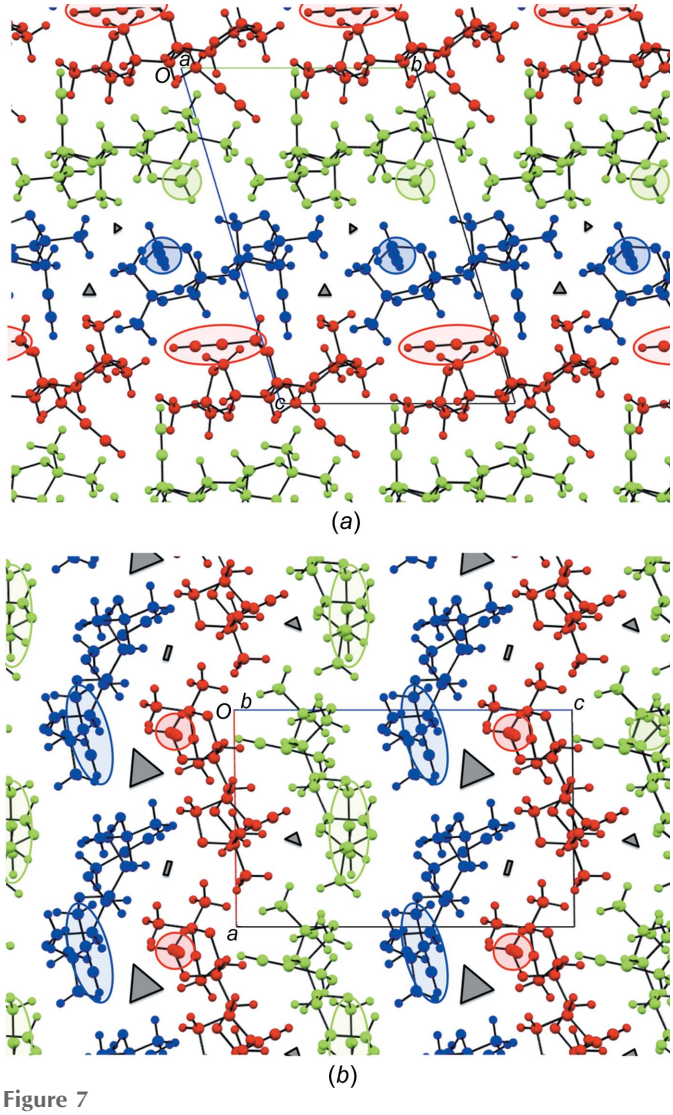

Figure 7
Crystal packing diagrams for compound **1**, showing the distinct layering of independent molecules *A* (green), *B* (blue) and *C* (red), as viewed in (*a*) along the *a* axis and in (*b*) along the *b* axis; the propargylic group in the 'tail' moiety of each molecule is circled in its respective colour to highlight the orthogonal directionality of the *C* (red) compared with the *A* (green) and *B* (blue) groups. Void spaces observed in the space-filling models are illustrated in cartoon form by dark-grey shapes with relative sizes drawn approximately to scale.

This situation was helped marginally when the E1.1, F1.1 and F2.1 interactions were considered as a whole (Fig S1 and Table 3). The E1.1 and F2.1 features showed a similarity not evident in F1.1; the bond to the distal C atom to which their donor methyl groups are attached is nearly unidirectional to the axis of the methyl C atom to acetylenic C atom trajectory, while in F1.1 it is at an acute angle (Fig. S1). Despite this observation, individual analyses showed that the more accurately measureable $D\cdots A$ distances increased in the order F2.1 $\leq$ E1.1 << F1.1, which was not the same as the order of the H$\cdots A$ distances (F2.1 $\leq$ F1.1 << E1.1) or the D—H$\cdots A$ angles (E1.1 < F2.1 << F1.1). On the other hand, for E1.1 there were no positive results but 71 negative results, and for F1.1 and F2.1, both recorded 76 results, with four and three, respectively, recorded as positive.

It was concluded from the lack of direct correlation between any of these trends, including intrastand and interstrand interactions, and the observed number of positive results, that the E1.1, F1.1 and F2.1 features are equally common to those in G, H and I, in the solid state. Again, the $D\cdots A$ distances encountered in the crystal structure of compound **1** must impose tight limitations that are not commonly met in structures within the CSD.

3.4.2.3. Analysis of structure codes for negative search results. Analysis of the breakdown of structure codes from each search (Table S2) showed relatively good coherence in the structure codes in the negative results for categories A1, A2 and C–I, but not for B1.1–B1.3. This outcome appears to mark a change from cyclic to acyclic O-atom acceptors. A similar lack of coherence was observed, *albeit* to a less dramatic extent because of fewer overall search results, for PFF J1.2–J1.4. Here it was noted that the donor H atom was part of a cyclic methylene group rather than from an exocyclic methyl group. Such factors were therefore important in interpreting the negative search results.

3.4.2.4. Analysis of structure codes for positive search results. As for positive results, there was a degree of coherence between structure codes within each of the search PFFs A1.1–A1.4, A2.1–A2.4, B1.1–B1.3 and C1.1–C1.4. The differences that were observed were readily attributable to variations in the attachments to the common acceptor atom in each set. In contrast, there was no overall coherence in the codes in the positive results between the first three categories, *i.e.* A1, A2 and B1 (Table S2). Initial thoughts of donor type or $D\cdots A$ distance as the cause were ruled out. Instead, a much more subtle feature appeared to be at play, namely, a different type of O-atom acceptor (Fig. S2), the influence of which was not as evident in the negative results. The similarities in positive result structure codes between A2, C and D results could then be explained by H$\cdots$C interactions in PFF C and D that were strongly influenced by the presence of the corresponding dioxolanyl-derived O—CH_2 attachment to the formal quaternary C-atom acceptors.

3.4.3. Analysis of loosely constrained *ConQuest* structural motif (CSM) search results. Despite the predominance of positive propargylic donor over acceptor interactions in strand assemblies in the crystal structure of compound **1**, the absolute sum of positive and negative donor interactions in each category from the study in Section 3.4.2 remained remarkably small. This prompted a more general search of the CSD for less constrained structural motifs (Fig. S3) that encompassed the main features of those already examined but focused on H$\cdots A$ (D1) and $D\cdots A$ (D2) contact distances, and D—H$\cdots A$ (ANG) angles.

3.4.3.1. CSD Index Numbers versus contact distances and angles. Simple scatterplots of the individual D1, D2 and ANG

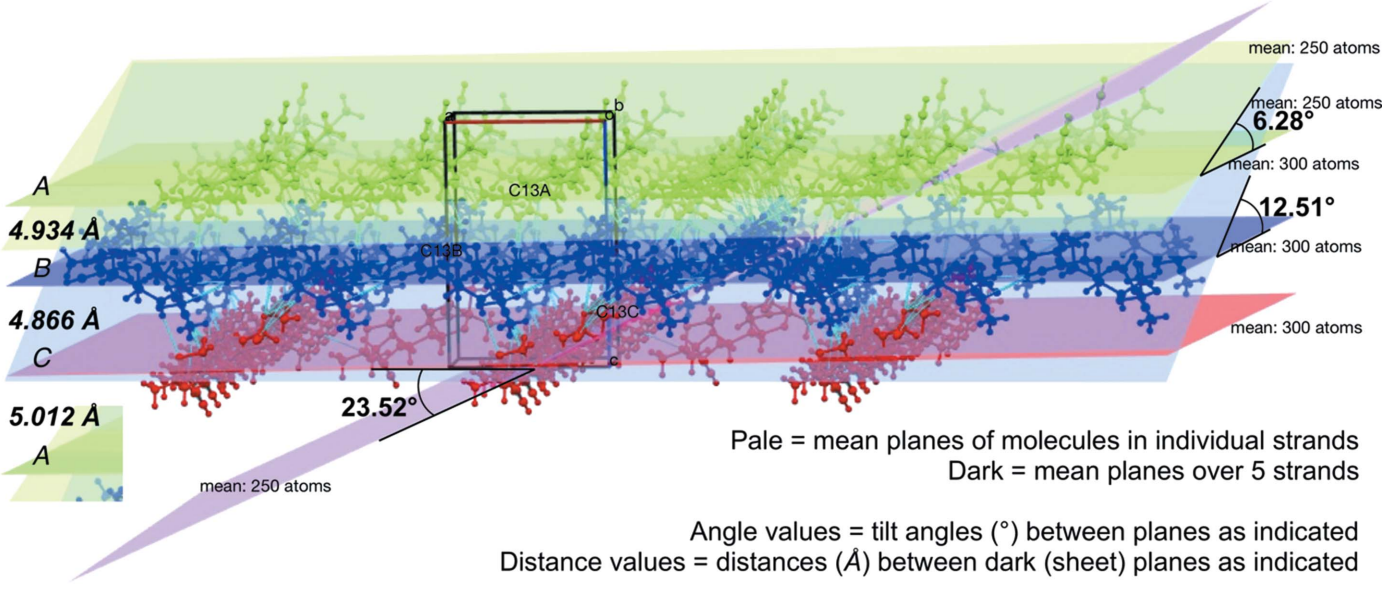

Figure 8
Mean planes of molecules *A* (green), *B* (blue) and *C* (red), as viewed slightly offset along the crystallographic *b* axis and recorded (*a*) in pale shades for individual molecular strands showing nonparallel but like planes for *A* and *B*, which are orthogonal to the angular plane of *C* strands, and (*b*) in dark shades for mean planes over five strands of each type, showing parallel but unequally spaced layers, which are repeated in the same order throughout.

values *versus* the CSD Index Numbers, with their respective search structure motifs (Fig. S3), revealed different cluster patterns in the distances, and to some degree contact angles, of each category, but no direct correlations, particularly between cases of multiple independent contacts within the one structure.

3.4.3.2. Contact distances and distance differences versus contact angles. Far more useful patterns emerged when scatterplots were constructed of D1 and D2 distances *versus* D—H$\cdots A$ (ANG) contact angles for the most populous donor acetylenic contacts to O (CSM1_R1) and C (CSM1_R4) acceptor atoms on the one hand, and acceptor acetylenic contacts at terminal C atoms (CSM1_R5) and C atoms adjacent to the terminal C atoms (CSM1_R6) by sp^3 C—H donors on the other [Fig. 10(*a*)].

All searches gave noticeable differences between D1 and D2 that became larger with increasing contact angles [upper portions of each plot in Fig. 10(*b*)]. Initial observations were codified by additionally recording scatterplots of D2–D1 values against contact angles for each contact motif [lower portions of each plot in Fig. 10(*b*)]. These showed a nonlinear progression of larger D2–D1 values with increasing contact angle. However, calculated trend lines for each set of the D1 and D2 distance curves unmasked stark differences for each search category in the contributions of D1 and D2. For example, at the two extremes, the CSM1_R1 interactions involved a relatively constant D2 ($D\cdots A$) distance and decreasing D1 (H$\cdots A$) distances, while those of the CSM1_R4 and CSM1_R6 interactions showed the opposite, with relatively constant D1 and decreasing D2 distances. In CSM1_R5, the D2 ($D\cdots A$) distances increased marginally, while the D1 (H$\cdots A$) distances decreased noticeably, with increasing D—H$\cdots A$ angle, indicating that both parameters contributed. Neither absolute magnitudes of D1 and D2 in each search category, which fell in the order CSM1_R1 < CSM1_R4 < CSM1_R5 $\simeq$ CSM1_R6, nor reported contact angles, which fell within four different ranges, could account for these observations. Instead, it was concluded that the type of acceptor atom (O *versus* C and terminal *versus* nonterminal acetylenic C) was probably responsible.

Despite these anomalies, when the scatterplots of the numerical difference (D2–D1) in contact distances *versus* contact angle in each category were plotted together, the correlation curves were virtually superposable [Fig. 10(*c*)]. Modelling studies revealed that very minor variations in the correlation curves were attributable to the different fixed C—H donor bond lengths (0.95–1.00 Å) embedded in each data set. Of the seven data points that could be regarded as outliers from these acknowledged trends, six were attributable to features in the CSD structures for just one compound, WUJWAC {(*R*)-1-[(4*S*,5*R*)-5-(hydroxymethyl)-2,2-dimethyl-1,3-dioxolan-4-yl]but-3-yn-1-ol} (Heinrich *et al.*, 2020) (1 × CSM1_R1, 1 × CSM1_R4, 3 × CSM1_R5 and 1 × CSM1_R6), and one attributable to one other compound, EHAKAZ

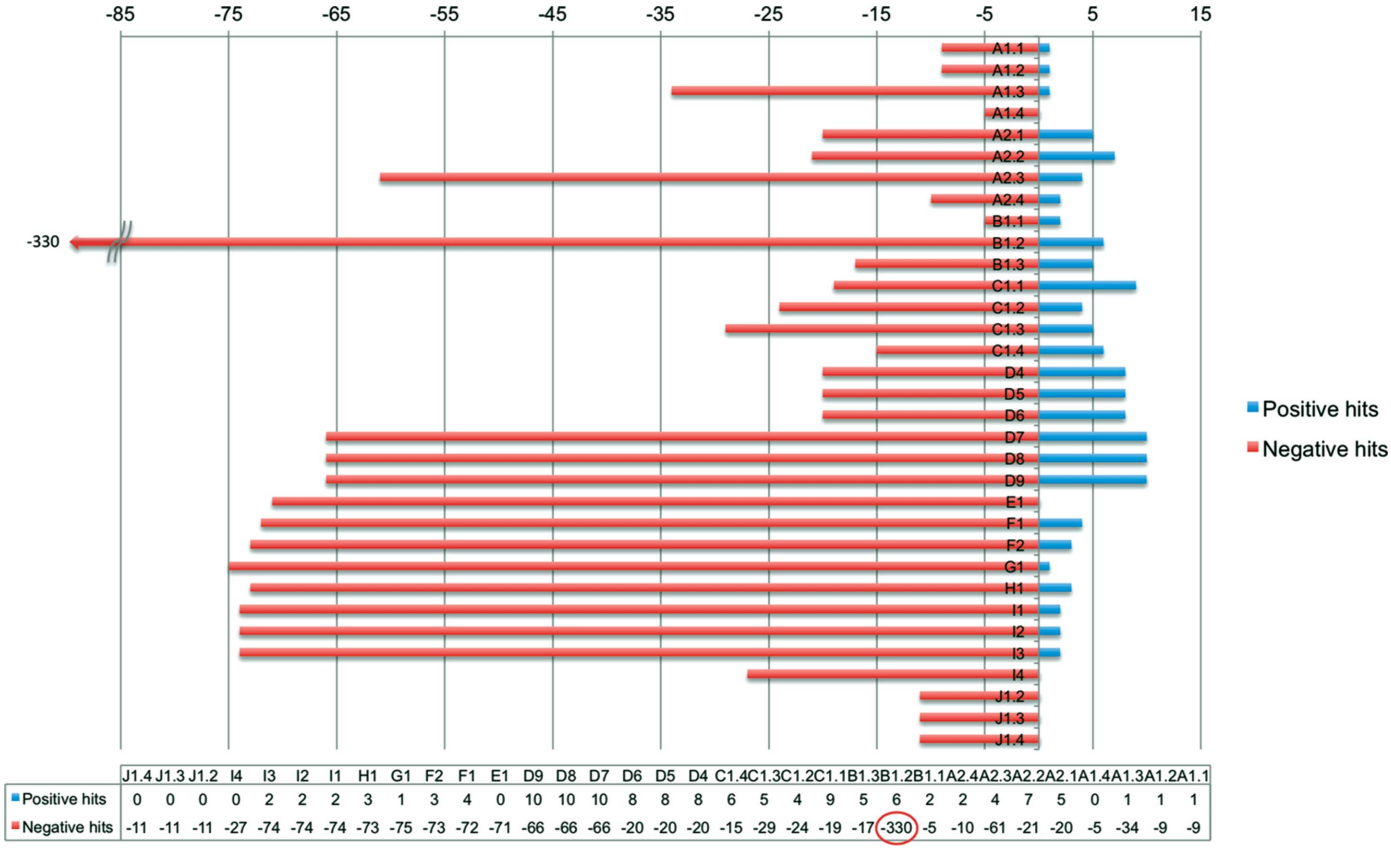

	J1.4	J1.3	J1.2	I4	I3	I2	I1	H1	G1	F2	F1	E1	D9	D8	D7	D6	D5	D4	C1.4	C1.3	C1.2	C1.1	B1.3	B1.2	B1.1	A2.4	A2.3	A2.2	A2.1	A1.4	A1.3	A1.2	A1.1
Positive hits	0	0	0	0	2	2	2	3	1	3	4	0	10	10	10	8	8	8	6	5	4	9	5	6	2	2	4	7	5	0	1	1	1
Negative hits	-11	-11	-11	-27	-74	-74	-74	-73	-75	-73	-72	-71	-66	-66	-66	-20	-20	-20	-15	-29	-24	-19	-17	-330	-5	-10	-61	-21	-20	-5	-34	-9	-9

Figure 9
A bar graph and table of the number of Positive (blue) and Negative (red) PFF results from each of the PFF searches.

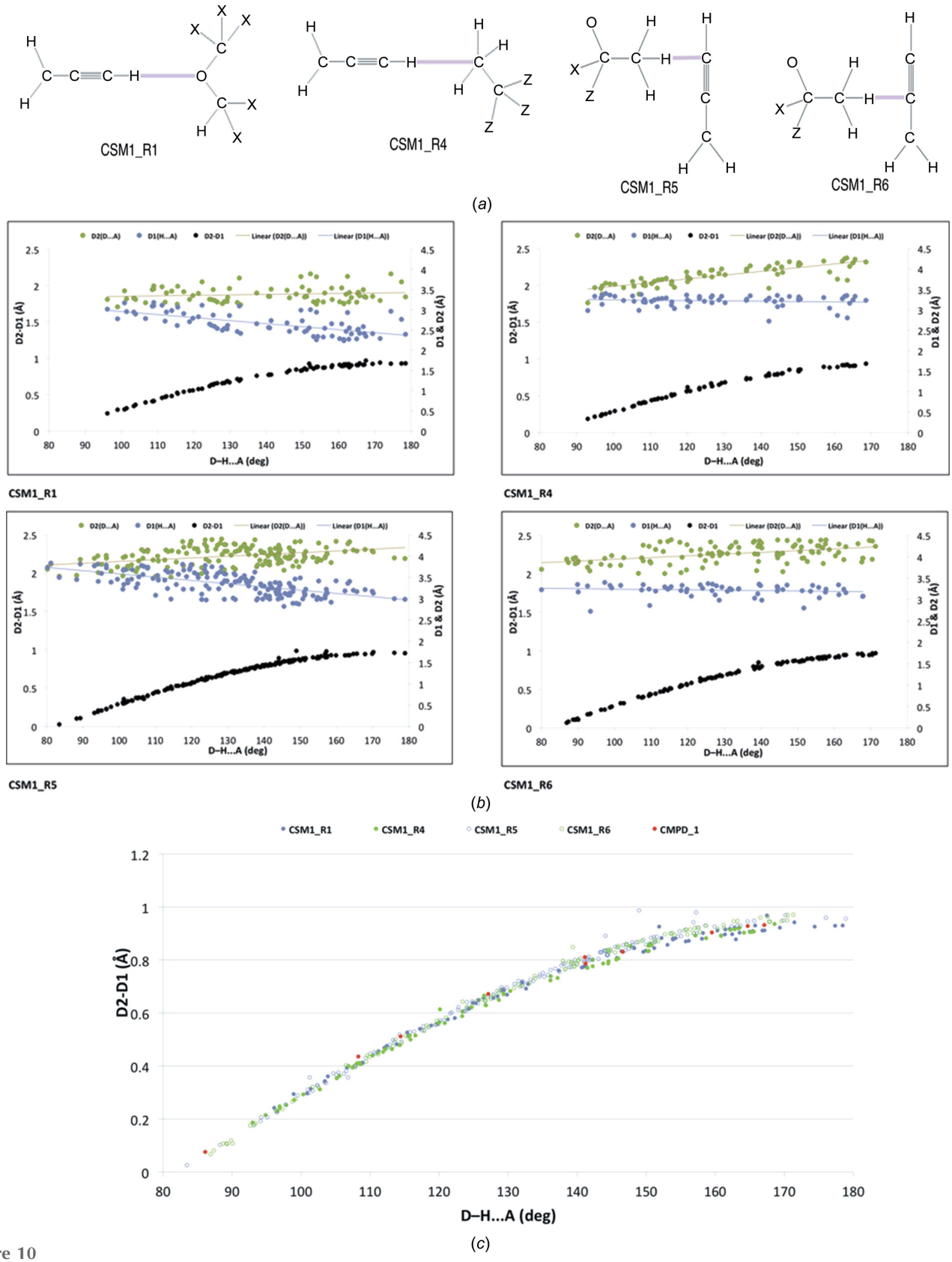

Figure 10
(*a*) *ConQuest* search motifs (CSMs) used to define searches of propargylic donor and acceptor interactions using loosely constrained distances (D1 and D2) and D—H···A angles (ANG). (*b*) Scatterplots of D1 (blue), D2 (green) and D2–D1 (black)(Å) values *versus* ANG (°) values for interactions in molecules satisfying criteria for *ConQuest* search motifs CSM1-R1, CSM1-R4, CSM1-R5 and CSM1-R6, including lines of best fit for the D1 and D2 results. (*c*) Overlay of the four scatterplots of D2–D1 values *versus* contact angle (ANG) from Fig. 10(*b*) (with changed marker shapes and colours), as well as related data points (in red) for relevant contacts in compound **1**.

[*N*-((1*R*,2*S*)-2-hydroxy-1-{(4*S*,4′*R*,5*S*)-2,2,2′,2′-tetramethyl-[4,4′-bi(1,3-dioxolan)]-5-yl}pent-4-yn-1-yl)acetamide] (Liu *et al.*, 2002) (CSM1_R5) (Fig. S4). Capture of the outliers was due to the liberal contact criteria inherent in the searches. The origins of their outlier properties could not be ascertained, although both molecules possess chirality and contain acetonide (dioxolanyl) and alcohol groups with multiple opportunities for additional competing inter- and intramolecular contacts. In particular, the hydroxyl groups of diol WUJWAC participitate in numerous strong hydrogen-bond interactions in the crystal, which probably drive the very complex array of weaker close contacts.

Relevant to the present study, an overlay of the corresponding measured data for representatives of contacts from the three crystallographic molecules *A*–*C* from compound **1** showed perfect superposition, with marker points [Fig. 10(*c*)] in red that were dispersed within the normal scatter across the full angular range of the data from the CDS searches.

To our knowledge, the type of comparisons just described have not been reported previously. They support the notion that acetylenic groups, particularly those originating in propargylic substituents, can participate in a wide range of weak but highly influential donor and acceptor interactions that are important in establishing crystal packing. These contacts can be mediated over a large range of contact angles, even within crystals of the one compound. It is valuable to recognize the high consistency of the correlations participated in by the terminal acetylenic component of the propargyl group, both as donor and as acceptor. As a corollary, rare departures from this norm can be an indication of additional powerful influences that might be present.

4. Summary and conclusion

A comprehensive single-crystal X-ray crystallographic analysis of 3,4-bis-*O*-propargyl-1,2:5,6-di-*O*-isopropylidene-D-mannitol, **1**, has revealed the presence of three independent molecules *A*–*C* in the unit cell, each differing in conformation. The molecules form a close-packed layered structure aligned in the *a* and *b* axes, with each layer comprising a well-ordered homogeneous array of like molecules. Tail-to-tail acetylenic C13—H13 donor and dioxolanyl O6 acceptor contacts are associated with strand-like substructures in each layer. Multiple, much weaker, interstrand contacts are associated with the packing of parallel strands in each sheet. Strands derived from molecules *A* and *B* align co-operatively with minimal contact, along the crystallographic *a* axis, while those from *C* align orthogonally along the *b* axis. A thorough systematic analysis of intra- and intermolecular interactions, including an examination of the geometric parameters associated with the observed close contacts, and consideration of the crystallographic planes, allows identification of the key interactions and provides strong support for the current understanding of weak hydrogen bonds and their description as a continuum of van der Waals contacts and electrostatic interactions. The evidence supports the notion that contact strength is best assessed in a *D*—H···*A* system from the *D*···*A* distance (D, Å), with a considerable flexibility in the *D*—H···*A* contact angle and the geometry about the acceptor, at least when *A* is oxygen or carbon.

Two secondary studies of the Cambridge Structural Database (CSD) using *Mercury* Crystal Packing Features (PFF) and *ConQuest* structural motifs, based on features identified in the crystals of compound **1** involving the propargyl group, add further insight into the value of **1** as a model for the study of weak interactions in the solid state. They give mathematical credence to the close correlation that exists in these *D*—H···*A* systems between the difference in distance between *D*···*A* and H···*A*, and the *D*—H···*A* angle, but point to different contributions that the *D*···*A* and H···*A* parameters can have in this correlation, depending upon the particular structural motif involved.

Overall, the studies described here provide new insight into factors involved in weak acetylenic H···*A* interactions and might well prove useful in guiding the design of chemoselective applications of such functional groups, especially where these are propagated in or close to the solid state.

Acknowledgements

This research did not receive any specific funding. X-Ray crystallographic analysis for this work was carried out at the Mark Wainwright Analytical Centre, UNSW, and was supported in part by infrastructure funding from the New South Wales Government as part of its co-investment in the National Collaborative Research Infrastructure Strategy. AIM was generously supported through a Research Fellowship Award from the University of Kerbala while on leave at UNSW. The authors declare no conflicts of interest.

Funding information

Funding for this research was provided by: National Collaborative Research Infrastructure Strategy (NCRIS). Open access publishing facilitated by University of New South Wales, as part of the Wiley–University of New South Wales agreement via the Council of Australian University Librarians.

References

Ahmed, A. M. A., Mohammed, A. I. & Read, R. W. (2020). *J. Fluor. Chem.* **234**, 109519.
Baillargeon, P., Lusser, T. & Dory, Y. L. (2014). *J. Crystallogr.* **2014**, 371629.
Bergman, R. G. (1973). *Acc. Chem. Res.* **6**, 25–31.
Bernstein, J. (2013). *Cryst. Growth Des.* **13**, 961–964.
Bruker (2016). *APEX3*, *SAINT* and *SADABS*. Bruker AXS Inc., Madison, Wisconsin, USA.
Capelli, S. C., Bürgi, H.-B., Dittrich, B., Grabowsky, S. & Jayatilaka, D. (2014). *IUCrJ*, **1**, 361–379.
Crich, D., Jayalath, P. & Hutton, T. K. (2006). *J. Org. Chem.* **71**, 3064–3070.
Desiraju, G. R. (1990). *J. Chem. Soc. Chem. Commun.* pp. 454–455.
Desiraju, G. R. (1991). *Acc. Chem. Res.* **24**, 290–296.
Desiraju, G. R. (1999). In *The Weak Hydrogen Bond*. Oxford University Press.
Desiraju, G. R. (2002). *Acc. Chem. Res.* **35**, 565–573.
Desiraju, G. R. (2005). *Chem. Commun.* pp. 2995–3001.
Desiraju, G. R. (2013). *J. Am. Chem. Soc.* **135**, 9952–9967.

Dolomanov, O. V., Bourhis, L. J., Gildea, R. J., Howard, J. A. K. & Puschmann, H. (2009). *J. Appl. Cryst.* **42**, 339–341.
Dunitz, J. D. & Gavezzotti, A. (2005). *Angew. Chem. Int. Ed.* **44**, 1766–1787.
Ghorai, S., Mukhopadhyay, R., Kundu, A. P. & Bhattacharjya, A. (2005). *Tetrahedron*, **61**, 2999–3012.
Groom, C. R., Bruno, I. J., Lightfoot, M. P. & Ward, S. C. (2016). *Acta Cryst.* B**72**, 171–179.
Hashmi, A. S. K., Wölfle, M., Teles, J. H. & Frey, W. (2007). *Synlett*, **2007**, 1747–1752.
Heinrich, M., Murphy, J. F., Ilg, M. K., Letort, A., Flasz, J. T., Philipps, P. & Fürstner, A. (2020). *J. Am. Chem. Soc.* **142**, 6409–6422.
Jayatilaka, D. & Dittrich, B. (2008). *Acta Cryst.* A**64**, 383–393.
Jones, C. R., Baruah, P. K., Thompson, A. L., Scheiner, S. & Smith, M. D. (2012). *J. Am. Chem. Soc.* **134**, 12064–12071.
Liu, K.-G., Yan, S., Wu, Y.-L. & Yao, Z.-J. (2002). *J. Org. Chem.* **67**, 6758–6763.
Macrae, C. F., Sovago, I., Cottrell, S. J., Galek, P. T. A., McCabe, P., Pidcock, E., Platings, M., Shields, G. P., Stevens, J. S., Towler, M. & Wood, P. A. (2020). *J. Appl. Cryst.* **53**, 226–235.
Manabe, S., Ueki, A. & Ito, Y. (2008). *Tetrahedron Lett.* **49**, 5159–5161.
Maurya, S. K. & Rana, R. (2017). *Beilstein J. Org. Chem.* **13**, 1106–1118.
Mohammed, A. I., Abboud, Z. H. & Alghanimi, A. H. O. (2012). *Tetrahedron Lett.* **53**, 5081–5083.
Parsons, S., Flack, H. D. & Wagner, T. (2013). *Acta Cryst.* B**69**, 249–259.
Pedireddi, V. R. & Desiraju, G. R. (1992). *J. Chem. Soc. Chem. Commun.* pp. 988–990.
Perez-Balderas, F., Morales-Sanfrutos, J., Hernandez-Mateo, F., Isac-García, J. & Santoyo-Gonzalez, F. (2009). *Eur. J. Org. Chem.* **2009**, 2441–2453.
Poloukhtine, A., Rassadin, V., Kuzmin, A. & Popik, V. V. (2010). *J. Org. Chem.* **75**, 5953–5962.
Rambabu, D., Bhavani, S., Swamy, N. K., Basaveswara Rao, M. V. & Pal, M. (2013). *Tetrahedron Lett.* **54**, 1169–1173.
Schwalbe, C. H. (2012). *Crystallogr. Rev.* **18**, 191–206.
Sheldrick, G. M. (2015*a*). *Acta Cryst.* A**71**, 3–8.
Sheldrick, G. M. (2015*b*). *Acta Cryst.* C**71**, 3–8.
Steiner, T. (2002). *Angew. Chem. Int. Ed.* **41**, 48–76.
Steiner, T. & Desiraju, G. R. (1998). *Chem. Commun.* pp. 891–892.
Taylor, R. & Kennard, O. (1982). *J. Am. Chem. Soc.* **104**, 5063–5070.
Taylor, R. & Kennard, O. (1984). *Acc. Chem. Res.* **17**, 320–326.
Woińska, M., Grabowsky, S., Dominiak, P. M., Woźniak, K. & Jayatilaka, D. (2016). *Sci. Adv.* **2**, e1600192.
Wu, Y.-T., Hayama, T., Baldridge, K. K., Linden, A. & Siegel, J. S. (2006). *J. Am. Chem. Soc.* **128**, 6870–6884.
Zhang, Y., Lao, W., Liu, Y., Yin, Y., Wu, J. & Huang, Z. (2001). *Polyhedron*, **20**, 1107–1113.

supporting information

Acta Cryst. (2022). C**78**, 629-646 [https://doi.org/10.1107/S205322962200897X]

3,4-Bis-*O*-propargyl-1,2:5,6-di-*O*-isopropylidene-D-mannitol: a study of multiple weak hydrogen bonds in the solid state

Adnan I. Mohammed, Mohan M. Bhadbhade and Roger W. Read

Computing details

Data collection: *APEX3* (Bruker, 2016); cell refinement: *SAINT* (Bruker, 2016); data reduction: *SAINT* (Bruker, 2016); program(s) used to solve structure: SHELXT (Sheldrick, 2015a); program(s) used to refine structure: *SHELXL* (Sheldrick, 2015b); molecular graphics: OLEX2 (Dolomanov *et al.*, 2009); software used to prepare material for publication: OLEX2 (Dolomanov *et al.*, 2009).

(1*R*,2*R*)-1,2-Bis[(*R*)-2,2-dimethyl-1,3-dioxolan-4-yl]-1,2-bis(prop-2-yn-1-yloxy)ethane

Crystal data

$C_{18}H_{26}O_6$
M_r = 338.39
Triclinic, *P*1
a = 9.4726 (4) Å
b = 10.3000 (5) Å
c = 15.3583 (7) Å
α = 73.378 (2)°
β = 88.382 (2)°
γ = 86.400 (2)°
V = 1432.94 (11) Å^3
Z = 3
F(000) = 546
D_x = 1.176 Mg m^{-3}
Mo *Kα* radiation, *λ* = 0.71073 Å
Cell parameters from 9994 reflections
θ = 2.6–30.4°
μ = 0.09 mm^{-1}
T = 150 K
Block, colourless
0.24 × 0.21 × 0.19 mm

Data collection

Bruker APEXII CCD diffractometer
Graphite monochromator
φ and *ω* scans
Absorption correction: multi-scan (SADABS; Bruker, 2016)
T_{min} = 0.679, T_{max} = 0.746
25389 measured reflections
8343 independent reflections
8134 reflections with $I > 2\sigma(I)$
R_{int} = 0.028
θ_{max} = 25.0°, θ_{min} = 2.6°
h = −11→11
k = −12→12
l = −16→18

Refinement

Refinement on F^2
Least-squares matrix: full
$R[F^2 > 2\sigma(F^2)]$ = 0.026
$wR(F^2)$ = 0.065
S = 1.02
8343 reflections
661 parameters
3 restraints
Hydrogen site location: inferred from neighbouring sites
H-atom parameters constrained
$w = 1/[\sigma^2(F_o^2) + (0.032P)^2 + 0.2227P]$ where $P = (F_o^2 + 2F_c^2)/3$
$(\Delta/\sigma)_{max} < 0.001$
$\Delta\rho_{max}$ = 0.21 e Å^{-3}
$\Delta\rho_{min}$ = −0.15 e Å^{-3}

Absolute structure: Flack *x* determined using 3228 quotients [(I+)-(I-)]/[(I+)+(I-)] (Parsons *et al.*, 2013)
Absolute structure parameter: 0.04 (17)

Special details

Geometry. All esds (except the esd in the dihedral angle between two l.s. planes) are estimated using the full covariance matrix. The cell esds are taken into account individually in the estimation of esds in distances, angles and torsion angles; correlations between esds in cell parameters are only used when they are defined by crystal symmetry. An approximate (isotropic) treatment of cell esds is used for estimating esds involving l.s. planes.

Refinement. A colourless block-like crystal of **1** with the dimensions 0.19 × 0.21 × 0.24 mm, selected under a polarizing microscope (Leica M165Z), was picked up on a MicroMount (MiTeGen, USA) consisting of a thin polymer tip with a wicking aperture. The X-ray diffraction measurements were carried out on a Bruker kappa-II CCD diffractometer at 150 K using IμS Incoatec Microfocus Source with Mo-Kα radiation (λ = 0.710723 Å). The single crystal, mounted on the goniometer using a cryo loop for intensity measurements, was coated with immersion oil type NVH and then quickly transferred to the cold nitrogen stream generated by an Oxford Cryostream 700 series. Symmetry-related absorption corrections using the program SADABS (Bruker, 2016) were applied and the data were corrected for Lorentz and polarisation effects using Bruker APEX3 software (Bruker, 2016). The structure was solved by program SHELXT (Sheldrick, 2015a) (with intrinsic phasing) and the full-matrix least-square refinements were carried out using SHELXL (Sheldrick, 2015b) through the OLEX2 (Dolomanov, 2009) software platform. Details of the experimental crystallographic data collected for compound **1** are summarized in Table 1. The non-hydrogen atoms were refined anisotropically.
The H atoms were not located in the difference Fourier map. Instead, the H atoms were placed geometrically and constrained according to their environment using different AFIX commands available in SHELXL (Sheldrick, 2015b) operating via the OLEX2 (Dolomanov, 2009) platform.

Fractional atomic coordinates and isotropic or equivalent isotropic displacement parameters (Å²)

	x	*y*	*z*	U_{iso}*/U_{eq}
O1A	0.5767 (2)	0.36428 (16)	0.40439 (11)	0.0489 (4)
O2A	0.54541 (15)	0.41366 (14)	0.25379 (10)	0.0330 (3)
O3A	0.24531 (14)	0.50233 (13)	0.28189 (9)	0.0290 (3)
O4A	0.32743 (15)	0.73829 (14)	0.32764 (10)	0.0317 (3)
O5A	0.15270 (14)	0.92079 (13)	0.17358 (10)	0.0289 (3)
O6A	−0.00610 (14)	0.85925 (14)	0.28710 (10)	0.0335 (3)
C1A	0.6383 (2)	0.3393 (2)	0.32429 (16)	0.0368 (5)
C2A	0.5095 (2)	0.4969 (2)	0.37928 (14)	0.0332 (5)
H2AA	0.565949	0.561019	0.398912	0.040*
H2AB	0.413939	0.496536	0.407191	0.040*
C3A	0.5001 (2)	0.5369 (2)	0.27551 (14)	0.0279 (4)
H3A	0.568748	0.607920	0.248585	0.034*
C4A	0.7862 (3)	0.3876 (3)	0.3084 (3)	0.0639 (8)
H4AA	0.822356	0.377996	0.250032	0.096*
H4AB	0.847564	0.333064	0.357378	0.096*
H4AC	0.784989	0.483173	0.307554	0.096*
C5A	0.6321 (3)	0.1904 (2)	0.33391 (19)	0.0485 (6)
H5AA	0.533783	0.164730	0.343942	0.073*
H5AB	0.689372	0.138090	0.385720	0.073*
H5AC	0.669065	0.171312	0.278332	0.073*
C6A	0.3554 (2)	0.58493 (18)	0.23527 (13)	0.0247 (4)
H6A	0.357882	0.582720	0.170576	0.030*

C7A	0.2188 (2)	0.3889 (2)	0.24967 (15)	0.0342 (5)
H7AA	0.141175	0.338975	0.286288	0.041*
H7AB	0.304508	0.326512	0.258799	0.041*
C8A	0.1808 (3)	0.4275 (2)	0.15384 (17)	0.0414 (6)
C9A	0.1549 (3)	0.4568 (3)	0.0760 (2)	0.0646 (8)
H9A	0.133910	0.480487	0.013034	0.078*
C10A	0.31561 (19)	0.73038 (19)	0.23687 (13)	0.0242 (4)
H10A	0.383700	0.792082	0.197112	0.029*
C11A	0.3807 (2)	0.8610 (2)	0.33579 (19)	0.0416 (6)
H11A	0.343471	0.878119	0.392624	0.050*
H11B	0.346433	0.937705	0.284276	0.050*
C12A	0.5352 (2)	0.8555 (2)	0.33670 (16)	0.0368 (5)
C13A	0.6594 (3)	0.8510 (3)	0.3393 (2)	0.0530 (7)
H13A	0.759777	0.847379	0.341310	0.064*
C14A	0.0180 (2)	0.9615 (2)	0.20448 (14)	0.0293 (4)
C15A	0.0487 (2)	0.7341 (2)	0.27351 (16)	0.0334 (5)
H15A	−0.025790	0.688674	0.251278	0.040*
H15B	0.087237	0.672175	0.330696	0.040*
C16A	0.1668 (2)	0.77518 (19)	0.20149 (14)	0.0261 (4)
H16A	0.149377	0.739783	0.148767	0.031*
C17A	0.0309 (3)	1.0948 (2)	0.22541 (18)	0.0429 (6)
H17A	−0.058732	1.120802	0.251044	0.064*
H17B	0.053129	1.164970	0.169404	0.064*
H17C	0.106602	1.085024	0.269395	0.064*
C18A	−0.0953 (2)	0.9680 (3)	0.13585 (18)	0.0456 (6)
H18A	−0.100003	0.878701	0.125695	0.068*
H18B	−0.072469	1.035035	0.078440	0.068*
H18C	−0.186838	0.994524	0.158902	0.068*
O1B	1.0876 (2)	1.16915 (16)	0.43913 (11)	0.0492 (4)
O2B	1.05781 (15)	1.13024 (14)	0.58974 (10)	0.0332 (3)
O3B	0.76846 (14)	1.04616 (13)	0.56368 (9)	0.0283 (3)
O4B	0.86447 (14)	0.79556 (13)	0.53706 (9)	0.0279 (3)
O5B	0.72215 (14)	0.62521 (13)	0.69482 (10)	0.0317 (3)
O6B	0.49602 (15)	0.71009 (15)	0.66106 (12)	0.0405 (4)
C1B	1.1431 (3)	1.1998 (2)	0.51572 (16)	0.0395 (5)
C2B	1.0363 (2)	1.0364 (2)	0.46958 (14)	0.0324 (5)
H2BA	1.102525	0.969835	0.451963	0.039*
H2BB	0.942460	1.034333	0.443360	0.039*
C3B	1.0256 (2)	1.0047 (2)	0.57313 (14)	0.0277 (4)
H3B	1.099290	0.932365	0.601679	0.033*
C4B	1.2967 (3)	1.1509 (3)	0.5300 (3)	0.0691 (9)
H4BA	1.306375	1.053342	0.536337	0.104*
H4BB	1.330406	1.168030	0.585202	0.104*
H4BC	1.352965	1.199614	0.477656	0.104*
C5B	1.1180 (3)	1.3501 (2)	0.50326 (19)	0.0525 (7)
H5BA	1.171484	1.400440	0.450053	0.079*
H5BB	1.149366	1.371919	0.557434	0.079*
H5BC	1.016911	1.375531	0.494201	0.079*

C6B	0.88139 (19)	0.96487 (18)	0.61587 (13)	0.0237 (4)
H6B	0.877626	0.978483	0.677820	0.028*
C7B	0.7308 (2)	1.1699 (2)	0.58671 (15)	0.0337 (5)
H7BA	0.670065	1.230020	0.538455	0.040*
H7BB	0.817704	1.217179	0.589249	0.040*
C8B	0.6558 (3)	1.1457 (2)	0.67389 (16)	0.0386 (5)
C9B	0.5940 (4)	1.1288 (3)	0.7426 (2)	0.0641 (9)
H9B	0.543620	1.115047	0.798606	0.077*
C10B	0.8592 (2)	0.81606 (19)	0.62558 (13)	0.0234 (4)
H10B	0.939195	0.760120	0.661727	0.028*
C11B	0.9412 (2)	0.6735 (2)	0.53223 (16)	0.0348 (5)
H11C	0.933231	0.664014	0.470227	0.042*
H11D	0.898297	0.594684	0.575257	0.042*
C12B	1.0903 (2)	0.6724 (2)	0.55378 (18)	0.0400 (5)
C13B	1.2085 (3)	0.6769 (3)	0.5753 (2)	0.0593 (8)
H13B	1.303346	0.680435	0.592636	0.071*
C14B	0.5836 (2)	0.5878 (2)	0.67922 (15)	0.0315 (5)
C15B	0.5864 (2)	0.8195 (2)	0.62337 (17)	0.0354 (5)
H15C	0.546644	0.905085	0.633850	0.042*
H15D	0.601566	0.833704	0.557340	0.042*
C16B	0.7218 (2)	0.77049 (19)	0.67517 (14)	0.0274 (4)
H16B	0.716709	0.795885	0.733386	0.033*
C17B	0.5916 (3)	0.5305 (3)	0.59954 (18)	0.0465 (6)
H17D	0.499693	0.496962	0.591521	0.070*
H17E	0.664017	0.455561	0.610530	0.070*
H17F	0.616309	0.601554	0.544548	0.070*
C18B	0.5279 (3)	0.4917 (3)	0.76485 (18)	0.0493 (6)
H18D	0.534131	0.531499	0.815363	0.074*
H18E	0.584436	0.405460	0.778480	0.074*
H18F	0.428998	0.475763	0.756414	0.074*
O1C	0.61167 (17)	0.75408 (17)	0.90309 (11)	0.0440 (4)
O2C	0.52196 (16)	0.76013 (14)	1.03885 (10)	0.0351 (3)
O3C	0.46869 (14)	1.05261 (14)	0.93971 (9)	0.0297 (3)
O4C	0.22924 (16)	1.01405 (14)	0.84581 (10)	0.0341 (3)
O5C	0.02811 (15)	1.17539 (14)	0.92172 (10)	0.0333 (3)
O6C	0.13492 (16)	1.37538 (13)	0.87903 (11)	0.0353 (3)
C1C	0.6185 (2)	0.6827 (2)	0.99641 (16)	0.0382 (5)
C2C	0.4691 (2)	0.8041 (2)	0.88441 (15)	0.0357 (5)
H2CA	0.415918	0.740689	0.861936	0.043*
H2CB	0.464849	0.894014	0.838436	0.043*
C3C	0.4087 (2)	0.81503 (19)	0.97665 (14)	0.0285 (4)
H3C	0.326164	0.756654	0.994319	0.034*
C4C	0.5704 (3)	0.5399 (2)	1.01459 (18)	0.0485 (6)
H4CA	0.473775	0.543536	0.992547	0.073*
H4CB	0.572606	0.494752	1.080061	0.073*
H4CC	0.633761	0.489083	0.982932	0.073*
C5C	0.7649 (3)	0.6880 (4)	1.0296 (2)	0.0662 (9)
H5CA	0.831584	0.633648	1.002461	0.099*

H5CB	0.766659	0.651628	1.095927	0.099*
H5CC	0.792168	0.782340	1.012066	0.099*
C6C	0.3656 (2)	0.95786 (19)	0.98242 (13)	0.0252 (4)
H6C	0.358711	0.954767	1.048069	0.030*
C7C	0.5798 (2)	1.0640 (2)	0.99815 (18)	0.0417 (6)
H7CA	0.659208	1.108934	0.960535	0.050*
H7CB	0.615105	0.971922	1.033336	0.050*
C8C	0.5331 (3)	1.1412 (2)	1.06105 (18)	0.0433 (6)
C9C	0.4966 (3)	1.2044 (3)	1.1112 (2)	0.0629 (8)
H9C	0.467075	1.255470	1.151724	0.075*
C10C	0.2229 (2)	1.00907 (19)	0.93945 (13)	0.0254 (4)
H10C	0.152132	0.942138	0.969985	0.031*
C11C	0.1055 (3)	0.9711 (2)	0.81240 (18)	0.0456 (6)
H11E	0.094424	1.020118	0.747139	0.055*
H11F	0.021046	0.995301	0.845263	0.055*
C12C	0.1132 (3)	0.8240 (2)	0.82386 (16)	0.0403 (5)
C13C	0.1198 (3)	0.7073 (3)	0.82963 (19)	0.0513 (6)
H13C	0.125184	0.613195	0.834289	0.062*
C14C	0.0083 (2)	1.3140 (2)	0.86833 (16)	0.0342 (5)
C15C	0.2465 (2)	1.27019 (19)	0.89366 (15)	0.0318 (5)
H15E	0.326336	1.291148	0.926667	0.038*
H15F	0.281872	1.256345	0.835503	0.038*
C16C	0.1723 (2)	1.14708 (19)	0.95107 (14)	0.0269 (4)
H16C	0.177314	1.143658	1.016649	0.032*
C17C	−0.0137 (3)	1.3202 (3)	0.77021 (18)	0.0522 (7)
H17G	0.069566	1.278060	0.747436	0.078*
H17H	−0.027508	1.415097	0.733914	0.078*
H17I	−0.097373	1.271299	0.765590	0.078*
C18C	−0.1132 (3)	1.3816 (3)	0.9080 (2)	0.0507 (6)
H18G	−0.200268	1.336462	0.905159	0.076*
H18H	−0.124911	1.477420	0.873184	0.076*
H18I	−0.093160	1.374728	0.971496	0.076*

Atomic displacement parameters (Å²)

	U^{11}	U^{22}	U^{33}	U^{12}	U^{13}	U^{23}
O1A	0.0747 (12)	0.0358 (9)	0.0325 (9)	0.0204 (8)	−0.0159 (8)	−0.0075 (7)
O2A	0.0375 (8)	0.0324 (8)	0.0288 (8)	0.0122 (6)	−0.0072 (6)	−0.0106 (6)
O3A	0.0346 (8)	0.0255 (7)	0.0274 (8)	−0.0074 (6)	0.0032 (6)	−0.0075 (6)
O4A	0.0343 (8)	0.0333 (8)	0.0312 (8)	−0.0004 (6)	−0.0042 (6)	−0.0150 (6)
O5A	0.0255 (7)	0.0239 (7)	0.0336 (8)	0.0025 (5)	0.0026 (6)	−0.0033 (6)
O6A	0.0278 (7)	0.0356 (8)	0.0326 (8)	0.0039 (6)	0.0045 (6)	−0.0042 (6)
C1A	0.0398 (12)	0.0343 (11)	0.0354 (12)	0.0114 (9)	−0.0134 (10)	−0.0101 (10)
C2A	0.0425 (12)	0.0278 (10)	0.0281 (11)	0.0067 (9)	−0.0107 (9)	−0.0071 (9)
C3A	0.0315 (11)	0.0247 (10)	0.0267 (11)	0.0028 (8)	−0.0029 (9)	−0.0066 (8)
C4A	0.0430 (15)	0.0520 (16)	0.093 (2)	0.0077 (12)	−0.0194 (15)	−0.0144 (16)
C5A	0.0562 (15)	0.0371 (13)	0.0508 (16)	0.0146 (11)	−0.0137 (13)	−0.0126 (12)
C6A	0.0288 (10)	0.0247 (10)	0.0190 (10)	−0.0003 (8)	0.0018 (8)	−0.0040 (8)

C7A	0.0399 (12)	0.0274 (11)	0.0366 (12)	−0.0057 (9)	−0.0024 (10)	−0.0101 (9)
C8A	0.0444 (13)	0.0408 (13)	0.0435 (15)	−0.0112 (10)	−0.0040 (11)	−0.0171 (11)
C9A	0.075 (2)	0.083 (2)	0.0406 (17)	−0.0277 (17)	−0.0117 (15)	−0.0193 (15)
C10A	0.0230 (10)	0.0241 (9)	0.0248 (10)	−0.0015 (7)	0.0016 (8)	−0.0062 (8)
C11A	0.0340 (12)	0.0390 (12)	0.0618 (16)	0.0053 (9)	−0.0117 (11)	−0.0309 (12)
C12A	0.0390 (13)	0.0278 (11)	0.0447 (14)	−0.0017 (9)	−0.0056 (10)	−0.0114 (10)
C13A	0.0352 (14)	0.0353 (13)	0.082 (2)	−0.0049 (10)	−0.0050 (13)	−0.0056 (13)
C14A	0.0242 (10)	0.0312 (10)	0.0296 (11)	0.0043 (8)	−0.0005 (8)	−0.0053 (9)
C15A	0.0257 (10)	0.0307 (11)	0.0403 (13)	−0.0019 (8)	0.0013 (9)	−0.0046 (9)
C16A	0.0275 (10)	0.0238 (10)	0.0262 (11)	−0.0016 (8)	−0.0008 (8)	−0.0055 (8)
C17A	0.0479 (14)	0.0345 (12)	0.0462 (14)	0.0075 (10)	0.0031 (11)	−0.0138 (11)
C18A	0.0346 (13)	0.0530 (15)	0.0448 (14)	0.0010 (10)	−0.0101 (11)	−0.0069 (12)
O1B	0.0763 (12)	0.0408 (9)	0.0311 (9)	−0.0230 (8)	0.0103 (9)	−0.0082 (7)
O2B	0.0403 (8)	0.0304 (7)	0.0300 (8)	−0.0115 (6)	0.0011 (7)	−0.0088 (6)
O3B	0.0317 (7)	0.0284 (7)	0.0229 (7)	0.0074 (6)	−0.0044 (6)	−0.0058 (6)
O4B	0.0285 (7)	0.0328 (7)	0.0248 (7)	0.0034 (6)	−0.0034 (6)	−0.0127 (6)
O5B	0.0290 (7)	0.0242 (7)	0.0412 (9)	−0.0035 (6)	−0.0046 (6)	−0.0074 (6)
O6B	0.0249 (7)	0.0372 (8)	0.0595 (11)	−0.0051 (6)	0.0014 (7)	−0.0138 (8)
C1B	0.0464 (13)	0.0377 (12)	0.0339 (12)	−0.0159 (10)	0.0074 (10)	−0.0070 (10)
C2B	0.0366 (11)	0.0319 (11)	0.0284 (11)	−0.0061 (9)	0.0054 (9)	−0.0077 (9)
C3B	0.0301 (10)	0.0247 (10)	0.0286 (11)	−0.0038 (8)	−0.0035 (9)	−0.0073 (8)
C4B	0.0400 (15)	0.071 (2)	0.093 (3)	−0.0154 (14)	0.0089 (16)	−0.0174 (18)
C5B	0.0757 (18)	0.0349 (13)	0.0469 (15)	−0.0200 (12)	0.0114 (14)	−0.0095 (11)
C6B	0.0266 (10)	0.0246 (9)	0.0186 (10)	0.0025 (8)	−0.0048 (8)	−0.0047 (8)
C7B	0.0415 (12)	0.0228 (10)	0.0322 (12)	0.0048 (8)	0.0054 (10)	−0.0025 (9)
C8B	0.0521 (14)	0.0247 (11)	0.0388 (13)	−0.0036 (10)	0.0081 (12)	−0.0091 (10)
C9B	0.099 (2)	0.0447 (15)	0.0530 (18)	−0.0189 (15)	0.0390 (18)	−0.0221 (13)
C10B	0.0235 (9)	0.0259 (9)	0.0211 (10)	0.0012 (7)	−0.0053 (8)	−0.0071 (8)
C11B	0.0307 (11)	0.0381 (12)	0.0418 (13)	0.0004 (9)	0.0010 (10)	−0.0218 (10)
C12B	0.0329 (13)	0.0333 (11)	0.0561 (15)	0.0033 (9)	0.0039 (11)	−0.0176 (11)
C13B	0.0287 (14)	0.0454 (15)	0.105 (3)	0.0034 (10)	−0.0077 (14)	−0.0237 (15)
C14B	0.0264 (10)	0.0310 (11)	0.0383 (12)	−0.0048 (8)	0.0004 (9)	−0.0112 (9)
C15B	0.0237 (10)	0.0289 (11)	0.0530 (15)	0.0005 (8)	−0.0030 (10)	−0.0110 (10)
C16B	0.0289 (10)	0.0242 (10)	0.0295 (11)	−0.0013 (8)	0.0005 (9)	−0.0086 (8)
C17B	0.0446 (14)	0.0544 (15)	0.0473 (15)	−0.0084 (11)	−0.0028 (12)	−0.0242 (13)
C18B	0.0512 (15)	0.0502 (15)	0.0462 (15)	−0.0180 (12)	0.0085 (12)	−0.0108 (12)
O1C	0.0450 (10)	0.0533 (10)	0.0343 (9)	0.0033 (8)	0.0074 (8)	−0.0155 (8)
O2C	0.0427 (8)	0.0354 (8)	0.0274 (8)	0.0150 (6)	−0.0067 (7)	−0.0123 (6)
O3C	0.0303 (7)	0.0322 (7)	0.0280 (8)	−0.0051 (6)	0.0008 (6)	−0.0101 (6)
O4C	0.0501 (9)	0.0298 (7)	0.0241 (7)	−0.0007 (7)	−0.0121 (7)	−0.0095 (6)
O5C	0.0305 (8)	0.0260 (7)	0.0391 (9)	0.0024 (6)	−0.0080 (6)	−0.0027 (6)
O6C	0.0409 (8)	0.0206 (7)	0.0436 (9)	0.0025 (6)	−0.0083 (7)	−0.0083 (6)
C1C	0.0404 (13)	0.0441 (13)	0.0321 (13)	0.0120 (10)	−0.0018 (10)	−0.0170 (10)
C2C	0.0470 (13)	0.0326 (11)	0.0291 (12)	0.0058 (9)	−0.0024 (10)	−0.0125 (10)
C3C	0.0337 (11)	0.0263 (10)	0.0244 (11)	0.0030 (8)	−0.0028 (9)	−0.0059 (8)
C4C	0.0623 (16)	0.0388 (13)	0.0438 (15)	0.0168 (11)	0.0012 (12)	−0.0153 (11)
C5C	0.0460 (16)	0.086 (2)	0.079 (2)	0.0208 (14)	−0.0141 (15)	−0.0476 (19)
C6C	0.0318 (10)	0.0254 (10)	0.0184 (9)	−0.0018 (8)	0.0011 (8)	−0.0061 (8)

C7C	0.0331 (12)	0.0444 (13)	0.0535 (15)	−0.0027 (10)	−0.0076 (11)	−0.0227 (12)
C8C	0.0467 (13)	0.0387 (13)	0.0458 (14)	0.0014 (10)	−0.0174 (11)	−0.0132 (12)
C9C	0.079 (2)	0.0647 (18)	0.0543 (17)	0.0127 (15)	−0.0203 (15)	−0.0341 (15)
C10C	0.0316 (10)	0.0217 (9)	0.0217 (10)	−0.0025 (8)	−0.0037 (8)	−0.0037 (8)
C11C	0.0631 (16)	0.0322 (12)	0.0450 (14)	0.0044 (11)	−0.0307 (12)	−0.0154 (11)
C12C	0.0513 (14)	0.0345 (13)	0.0360 (13)	−0.0007 (10)	−0.0168 (11)	−0.0104 (10)
C13C	0.0646 (17)	0.0323 (13)	0.0586 (17)	−0.0040 (11)	−0.0202 (14)	−0.0133 (12)
C14C	0.0403 (12)	0.0233 (10)	0.0375 (12)	0.0031 (9)	−0.0108 (10)	−0.0065 (9)
C15C	0.0345 (11)	0.0217 (10)	0.0379 (12)	0.0001 (8)	−0.0049 (9)	−0.0063 (9)
C16C	0.0287 (10)	0.0263 (10)	0.0248 (10)	0.0006 (8)	−0.0045 (8)	−0.0059 (8)
C17C	0.0766 (19)	0.0367 (13)	0.0420 (15)	0.0062 (12)	−0.0240 (14)	−0.0088 (11)
C18C	0.0444 (14)	0.0398 (13)	0.0703 (19)	0.0097 (11)	−0.0086 (13)	−0.0213 (13)

Geometric parameters (Å, º)

O1A—C1A	1.429 (3)	C6B—C10B	1.524 (2)
O1A—C2A	1.423 (3)	C7B—H7BA	0.9900
O2A—C1A	1.424 (3)	C7B—H7BB	0.9900
O2A—C3A	1.440 (2)	C7B—C8B	1.462 (3)
O3A—C6A	1.430 (2)	C8B—C9B	1.166 (3)
O3A—C7A	1.431 (2)	C9B—H9B	0.9500
O4A—C10A	1.427 (2)	C10B—H10B	1.0000
O4A—C11A	1.429 (2)	C10B—C16B	1.520 (3)
O5A—C14A	1.429 (2)	C11B—H11C	0.9900
O5A—C16A	1.436 (2)	C11B—H11D	0.9900
O6A—C14A	1.422 (3)	C11B—C12B	1.458 (3)
O6A—C15A	1.428 (2)	C12B—C13B	1.184 (4)
C1A—C4A	1.506 (4)	C13B—H13B	0.9500
C1A—C5A	1.503 (3)	C14B—C17B	1.502 (3)
C2A—H2AA	0.9900	C14B—C18B	1.506 (3)
C2A—H2AB	0.9900	C15B—H15C	0.9900
C2A—C3A	1.532 (3)	C15B—H15D	0.9900
C3A—H3A	1.0000	C15B—C16B	1.510 (3)
C3A—C6A	1.514 (3)	C16B—H16B	1.0000
C4A—H4AA	0.9800	C17B—H17D	0.9800
C4A—H4AB	0.9800	C17B—H17E	0.9800
C4A—H4AC	0.9800	C17B—H17F	0.9800
C5A—H5AA	0.9800	C18B—H18D	0.9800
C5A—H5AB	0.9800	C18B—H18E	0.9800
C5A—H5AC	0.9800	C18B—H18F	0.9800
C6A—H6A	1.0000	O1C—C1C	1.413 (3)
C6A—C10A	1.529 (2)	O1C—C2C	1.422 (3)
C7A—H7AA	0.9900	O2C—C1C	1.439 (2)
C7A—H7AB	0.9900	O2C—C3C	1.434 (3)
C7A—C8A	1.460 (3)	O3C—C6C	1.433 (2)
C8A—C9A	1.176 (4)	O3C—C7C	1.434 (3)
C9A—H9A	0.9500	O4C—C10C	1.424 (2)
C10A—H10A	1.0000	O4C—C11C	1.436 (3)

C10A—C16A	1.521 (3)	O5C—C14C	1.432 (3)
C11A—H11A	0.9900	O5C—C16C	1.436 (2)
C11A—H11B	0.9900	O6C—C14C	1.425 (3)
C11A—C12A	1.461 (3)	O6C—C15C	1.440 (3)
C12A—C13A	1.176 (3)	C1C—C4C	1.513 (3)
C13A—H13A	0.9500	C1C—C5C	1.500 (4)
C14A—C17A	1.509 (3)	C2C—H2CA	0.9900
C14A—C18A	1.510 (3)	C2C—H2CB	0.9900
C15A—H15A	0.9900	C2C—C3C	1.544 (3)
C15A—H15B	0.9900	C3C—H3C	1.0000
C15A—C16A	1.541 (3)	C3C—C6C	1.528 (3)
C16A—H16A	1.0000	C4C—H4CA	0.9800
C17A—H17A	0.9800	C4C—H4CB	0.9800
C17A—H17B	0.9800	C4C—H4CC	0.9800
C17A—H17C	0.9800	C5C—H5CA	0.9800
C18A—H18A	0.9800	C5C—H5CB	0.9800
C18A—H18B	0.9800	C5C—H5CC	0.9800
C18A—H18C	0.9800	C6C—H6C	1.0000
O1B—C1B	1.424 (3)	C6C—C10C	1.518 (3)
O1B—C2B	1.424 (2)	C7C—H7CA	0.9900
O2B—C1B	1.419 (2)	C7C—H7CB	0.9900
O2B—C3B	1.439 (2)	C7C—C8C	1.460 (3)
O3B—C6B	1.428 (2)	C8C—C9C	1.174 (4)
O3B—C7B	1.439 (2)	C9C—H9C	0.9500
O4B—C10B	1.433 (2)	C10C—H10C	1.0000
O4B—C11B	1.432 (2)	C10C—C16C	1.529 (3)
O5B—C14B	1.436 (2)	C11C—H11E	0.9900
O5B—C16B	1.439 (2)	C11C—H11F	0.9900
O6B—C14B	1.426 (3)	C11C—C12C	1.472 (3)
O6B—C15B	1.435 (3)	C12C—C13C	1.177 (3)
C1B—C4B	1.510 (4)	C13C—H13C	0.9500
C1B—C5B	1.509 (3)	C14C—C17C	1.510 (3)
C2B—H2BA	0.9900	C14C—C18C	1.511 (3)
C2B—H2BB	0.9900	C15C—H15E	0.9900
C2B—C3B	1.531 (3)	C15C—H15F	0.9900
C3B—H3B	1.0000	C15C—C16C	1.522 (3)
C3B—C6B	1.527 (3)	C16C—H16C	1.0000
C4B—H4BA	0.9800	C17C—H17G	0.9800
C4B—H4BB	0.9800	C17C—H17H	0.9800
C4B—H4BC	0.9800	C17C—H17I	0.9800
C5B—H5BA	0.9800	C18C—H18G	0.9800
C5B—H5BB	0.9800	C18C—H18H	0.9800
C5B—H5BC	0.9800	C18C—H18I	0.9800
C6B—H6B	1.0000		

C2A—O1A—C1A	107.92 (17)	C8B—C7B—H7BB	109.1
C1A—O2A—C3A	106.52 (15)	C9B—C8B—C7B	178.5 (3)
C6A—O3A—C7A	115.53 (14)	C8B—C9B—H9B	180.0

C10A—O4A—C11A	115.33 (16)	O4B—C10B—C6B	108.79 (15)
C14A—O5A—C16A	108.14 (13)	O4B—C10B—H10B	108.1
C14A—O6A—C15A	106.41 (15)	O4B—C10B—C16B	111.48 (15)
O1A—C1A—C4A	111.1 (2)	C6B—C10B—H10B	108.1
O1A—C1A—C5A	107.81 (19)	C16B—C10B—C6B	112.16 (15)
O2A—C1A—O1A	103.83 (16)	C16B—C10B—H10B	108.1
O2A—C1A—C4A	111.7 (2)	O4B—C11B—H11C	109.2
O2A—C1A—C5A	108.97 (18)	O4B—C11B—H11D	109.2
C5A—C1A—C4A	113.0 (2)	O4B—C11B—C12B	112.20 (16)
O1A—C2A—H2AA	110.7	H11C—C11B—H11D	107.9
O1A—C2A—H2AB	110.7	C12B—C11B—H11C	109.2
O1A—C2A—C3A	105.18 (16)	C12B—C11B—H11D	109.2
H2AA—C2A—H2AB	108.8	C13B—C12B—C11B	175.3 (2)
C3A—C2A—H2AA	110.7	C12B—C13B—H13B	180.0
C3A—C2A—H2AB	110.7	O5B—C14B—C17B	108.60 (16)
O2A—C3A—C2A	103.38 (16)	O5B—C14B—C18B	109.72 (19)
O2A—C3A—H3A	109.3	O6B—C14B—O5B	105.49 (15)
O2A—C3A—C6A	108.86 (16)	O6B—C14B—C17B	111.8 (2)
C2A—C3A—H3A	109.3	O6B—C14B—C18B	107.34 (17)
C6A—C3A—C2A	116.55 (16)	C17B—C14B—C18B	113.59 (19)
C6A—C3A—H3A	109.3	O6B—C15B—H15C	111.3
C1A—C4A—H4AA	109.5	O6B—C15B—H15D	111.3
C1A—C4A—H4AB	109.5	O6B—C15B—C16B	102.53 (17)
C1A—C4A—H4AC	109.5	H15C—C15B—H15D	109.2
H4AA—C4A—H4AB	109.5	C16B—C15B—H15C	111.3
H4AA—C4A—H4AC	109.5	C16B—C15B—H15D	111.3
H4AB—C4A—H4AC	109.5	O5B—C16B—C10B	107.92 (15)
C1A—C5A—H5AA	109.5	O5B—C16B—C15B	103.46 (15)
C1A—C5A—H5AB	109.5	O5B—C16B—H16B	109.4
C1A—C5A—H5AC	109.5	C10B—C16B—H16B	109.4
H5AA—C5A—H5AB	109.5	C15B—C16B—C10B	117.00 (18)
H5AA—C5A—H5AC	109.5	C15B—C16B—H16B	109.4
H5AB—C5A—H5AC	109.5	C14B—C17B—H17D	109.5
O3A—C6A—C3A	113.10 (16)	C14B—C17B—H17E	109.5
O3A—C6A—H6A	108.3	C14B—C17B—H17F	109.5
O3A—C6A—C10A	107.26 (14)	H17D—C17B—H17E	109.5
C3A—C6A—H6A	108.3	H17D—C17B—H17F	109.5
C3A—C6A—C10A	111.46 (16)	H17E—C17B—H17F	109.5
C10A—C6A—H6A	108.3	C14B—C18B—H18D	109.5
O3A—C7A—H7AA	108.9	C14B—C18B—H18E	109.5
O3A—C7A—H7AB	108.9	C14B—C18B—H18F	109.5
O3A—C7A—C8A	113.23 (18)	H18D—C18B—H18E	109.5
H7AA—C7A—H7AB	107.7	H18D—C18B—H18F	109.5
C8A—C7A—H7AA	108.9	H18E—C18B—H18F	109.5
C8A—C7A—H7AB	108.9	C1C—O1C—C2C	107.30 (16)
C9A—C8A—C7A	177.6 (3)	C3C—O2C—C1C	107.38 (15)
C8A—C9A—H9A	180.0	C6C—O3C—C7C	114.70 (16)
O4A—C10A—C6A	108.87 (16)	C10C—O4C—C11C	114.88 (17)

O4A—C10A—H10A	108.7	C14C—O5C—C16C	109.83 (15)
O4A—C10A—C16A	110.70 (14)	C14C—O6C—C15C	106.49 (14)
C6A—C10A—H10A	108.7	O1C—C1C—O2C	103.88 (17)
C16A—C10A—C6A	111.23 (15)	O1C—C1C—C4C	111.61 (19)
C16A—C10A—H10A	108.7	O1C—C1C—C5C	109.0 (2)
O4A—C11A—H11A	109.2	O2C—C1C—C4C	109.82 (18)
O4A—C11A—H11B	109.2	O2C—C1C—C5C	108.56 (18)
O4A—C11A—C12A	112.26 (17)	C5C—C1C—C4C	113.5 (2)
H11A—C11A—H11B	107.9	O1C—C2C—H2CA	110.9
C12A—C11A—H11A	109.2	O1C—C2C—H2CB	110.9
C12A—C11A—H11B	109.2	O1C—C2C—C3C	104.41 (18)
C13A—C12A—C11A	178.6 (3)	H2CA—C2C—H2CB	108.9
C12A—C13A—H13A	180.0	C3C—C2C—H2CA	110.9
O5A—C14A—C17A	108.41 (16)	C3C—C2C—H2CB	110.9
O5A—C14A—C18A	110.89 (17)	O2C—C3C—C2C	103.92 (16)
O6A—C14A—O5A	103.97 (15)	O2C—C3C—H3C	109.3
O6A—C14A—C17A	108.75 (17)	O2C—C3C—C6C	108.41 (15)
O6A—C14A—C18A	111.37 (17)	C2C—C3C—H3C	109.3
C17A—C14A—C18A	113.02 (19)	C6C—C3C—C2C	116.41 (17)
O6A—C15A—H15A	110.9	C6C—C3C—H3C	109.3
O6A—C15A—H15B	110.9	C1C—C4C—H4CA	109.5
O6A—C15A—C16A	104.47 (15)	C1C—C4C—H4CB	109.5
H15A—C15A—H15B	108.9	C1C—C4C—H4CC	109.5
C16A—C15A—H15A	110.9	H4CA—C4C—H4CB	109.5
C16A—C15A—H15B	110.9	H4CA—C4C—H4CC	109.5
O5A—C16A—C10A	108.88 (15)	H4CB—C4C—H4CC	109.5
O5A—C16A—C15A	103.72 (15)	C1C—C5C—H5CA	109.5
O5A—C16A—H16A	109.9	C1C—C5C—H5CB	109.5
C10A—C16A—C15A	114.47 (17)	C1C—C5C—H5CC	109.5
C10A—C16A—H16A	109.9	H5CA—C5C—H5CB	109.5
C15A—C16A—H16A	109.9	H5CA—C5C—H5CC	109.5
C14A—C17A—H17A	109.5	H5CB—C5C—H5CC	109.5
C14A—C17A—H17B	109.5	O3C—C6C—C3C	111.51 (15)
C14A—C17A—H17C	109.5	O3C—C6C—H6C	108.1
H17A—C17A—H17B	109.5	O3C—C6C—C10C	108.76 (15)
H17A—C17A—H17C	109.5	C3C—C6C—H6C	108.1
H17B—C17A—H17C	109.5	C10C—C6C—C3C	112.04 (16)
C14A—C18A—H18A	109.5	C10C—C6C—H6C	108.1
C14A—C18A—H18B	109.5	O3C—C7C—H7CA	109.1
C14A—C18A—H18C	109.5	O3C—C7C—H7CB	109.1
H18A—C18A—H18B	109.5	O3C—C7C—C8C	112.40 (19)
H18A—C18A—H18C	109.5	H7CA—C7C—H7CB	107.9
H18B—C18A—H18C	109.5	C8C—C7C—H7CA	109.1
C1B—O1B—C2B	107.75 (16)	C8C—C7C—H7CB	109.1
C1B—O2B—C3B	106.77 (15)	C9C—C8C—C7C	179.2 (3)
C6B—O3B—C7B	114.46 (15)	C8C—C9C—H9C	180.0
C11B—O4B—C10B	114.60 (16)	O4C—C10C—C6C	109.45 (15)
C14B—O5B—C16B	109.25 (15)	O4C—C10C—H10C	107.8

C14B—O6B—C15B	106.73 (14)	O4C—C10C—C16C	110.75 (16)
O1B—C1B—C4B	111.2 (2)	C6C—C10C—H10C	107.8
O1B—C1B—C5B	108.4 (2)	C6C—C10C—C16C	112.93 (16)
O2B—C1B—O1B	104.31 (16)	C16C—C10C—H10C	107.8
O2B—C1B—C4B	111.1 (2)	O4C—C11C—H11E	109.2
O2B—C1B—C5B	108.03 (18)	O4C—C11C—H11F	109.2
C5B—C1B—C4B	113.3 (2)	O4C—C11C—C12C	112.1 (2)
O1B—C2B—H2BA	110.7	H11E—C11C—H11F	107.9
O1B—C2B—H2BB	110.7	C12C—C11C—H11E	109.2
O1B—C2B—C3B	105.13 (16)	C12C—C11C—H11F	109.2
H2BA—C2B—H2BB	108.8	C13C—C12C—C11C	177.6 (3)
C3B—C2B—H2BA	110.7	C12C—C13C—H13C	180.0
C3B—C2B—H2BB	110.7	O5C—C14C—C17C	109.69 (17)
O2B—C3B—C2B	103.53 (15)	O5C—C14C—C18C	109.09 (19)
O2B—C3B—H3B	109.5	O6C—C14C—O5C	105.14 (17)
O2B—C3B—C6B	108.31 (15)	O6C—C14C—C17C	111.3 (2)
C2B—C3B—H3B	109.5	O6C—C14C—C18C	108.26 (17)
C6B—C3B—C2B	116.29 (17)	C17C—C14C—C18C	113.0 (2)
C6B—C3B—H3B	109.5	O6C—C15C—H15E	111.3
C1B—C4B—H4BA	109.5	O6C—C15C—H15F	111.3
C1B—C4B—H4BB	109.5	O6C—C15C—C16C	102.10 (16)
C1B—C4B—H4BC	109.5	H15E—C15C—H15F	109.2
H4BA—C4B—H4BB	109.5	C16C—C15C—H15E	111.3
H4BA—C4B—H4BC	109.5	C16C—C15C—H15F	111.3
H4BB—C4B—H4BC	109.5	O5C—C16C—C10C	108.28 (15)
C1B—C5B—H5BA	109.5	O5C—C16C—C15C	103.24 (16)
C1B—C5B—H5BB	109.5	O5C—C16C—H16C	109.4
C1B—C5B—H5BC	109.5	C10C—C16C—H16C	109.4
H5BA—C5B—H5BB	109.5	C15C—C16C—C10C	116.94 (16)
H5BA—C5B—H5BC	109.5	C15C—C16C—H16C	109.4
H5BB—C5B—H5BC	109.5	C14C—C17C—H17G	109.5
O3B—C6B—C3B	111.80 (15)	C14C—C17C—H17H	109.5
O3B—C6B—H6B	108.4	C14C—C17C—H17I	109.5
O3B—C6B—C10B	108.72 (15)	H17G—C17C—H17H	109.5
C3B—C6B—H6B	108.4	H17G—C17C—H17I	109.5
C10B—C6B—C3B	111.05 (15)	H17H—C17C—H17I	109.5
C10B—C6B—H6B	108.4	C14C—C18C—H18G	109.5
O3B—C7B—H7BA	109.1	C14C—C18C—H18H	109.5
O3B—C7B—H7BB	109.1	C14C—C18C—H18I	109.5
O3B—C7B—C8B	112.38 (16)	H18G—C18C—H18H	109.5
H7BA—C7B—H7BB	107.9	H18G—C18C—H18I	109.5
C8B—C7B—H7BA	109.1	H18H—C18C—H18I	109.5

O1A—C2A—C3A—O2A	8.0 (2)	C3B—O2B—C1B—C5B	151.4 (2)
O1A—C2A—C3A—C6A	127.32 (18)	C3B—C6B—C10B—O4B	−61.0 (2)
O2A—C3A—C6A—O3A	71.97 (19)	C3B—C6B—C10B—C16B	175.18 (16)
O2A—C3A—C6A—C10A	−167.08 (14)	C6B—O3B—C7B—C8B	−72.8 (2)
O3A—C6A—C10A—O4A	69.86 (18)	C6B—C10B—C16B—O5B	−170.17 (16)

O3A—C6A—C10A—C16A	−52.4 (2)	C6B—C10B—C16B—C15B	73.8 (2)
O4A—C10A—C16A—O5A	79.35 (18)	C7B—O3B—C6B—C3B	−88.03 (18)
O4A—C10A—C16A—C15A	−36.2 (2)	C7B—O3B—C6B—C10B	149.01 (15)
O6A—C15A—C16A—O5A	−7.5 (2)	C10B—O4B—C11B—C12B	−63.2 (2)
O6A—C15A—C16A—C10A	111.01 (18)	C11B—O4B—C10B—C6B	138.17 (16)
C1A—O1A—C2A—C3A	14.6 (2)	C11B—O4B—C10B—C16B	−97.64 (19)
C1A—O2A—C3A—C2A	−27.7 (2)	C14B—O5B—C16B—C10B	−139.19 (17)
C1A—O2A—C3A—C6A	−152.24 (16)	C14B—O5B—C16B—C15B	−14.6 (2)
C2A—O1A—C1A—O2A	−31.9 (2)	C14B—O6B—C15B—C16B	−35.9 (2)
C2A—O1A—C1A—C4A	88.2 (2)	C15B—O6B—C14B—O5B	27.4 (2)
C2A—O1A—C1A—C5A	−147.4 (2)	C15B—O6B—C14B—C17B	−90.5 (2)
C2A—C3A—C6A—O3A	−44.4 (2)	C15B—O6B—C14B—C18B	144.34 (19)
C2A—C3A—C6A—C10A	76.6 (2)	C16B—O5B—C14B—O6B	−7.0 (2)
C3A—O2A—C1A—O1A	37.2 (2)	C16B—O5B—C14B—C17B	112.93 (19)
C3A—O2A—C1A—C4A	−82.5 (2)	C16B—O5B—C14B—C18B	−122.38 (18)
C3A—O2A—C1A—C5A	151.93 (18)	O1C—C2C—C3C—O2C	−4.1 (2)
C3A—C6A—C10A—O4A	−54.44 (19)	O1C—C2C—C3C—C6C	115.03 (19)
C3A—C6A—C10A—C16A	−176.68 (15)	O2C—C3C—C6C—O3C	73.42 (19)
C6A—O3A—C7A—C8A	−58.6 (2)	O2C—C3C—C6C—C10C	−164.40 (15)
C6A—C10A—C16A—O5A	−159.48 (15)	O3C—C6C—C10C—O4C	63.06 (18)
C6A—C10A—C16A—C15A	85.0 (2)	O3C—C6C—C10C—C16C	−60.82 (19)
C7A—O3A—C6A—C3A	−88.7 (2)	O4C—C10C—C16C—O5C	66.19 (19)
C7A—O3A—C6A—C10A	148.04 (17)	O4C—C10C—C16C—C15C	−49.8 (2)
C10A—O4A—C11A—C12A	−86.2 (2)	O6C—C15C—C16C—O5C	29.57 (19)
C11A—O4A—C10A—C6A	142.53 (16)	O6C—C15C—C16C—C10C	148.32 (17)
C11A—O4A—C10A—C16A	−94.91 (19)	C1C—O1C—C2C—C3C	25.1 (2)
C14A—O5A—C16A—C10A	−137.44 (16)	C1C—O2C—C3C—C2C	−17.9 (2)
C14A—O5A—C16A—C15A	−15.2 (2)	C1C—O2C—C3C—C6C	−142.36 (16)
C14A—O6A—C15A—C16A	27.5 (2)	C2C—O1C—C1C—O2C	−36.6 (2)
C15A—O6A—C14A—O5A	−37.32 (19)	C2C—O1C—C1C—C4C	81.6 (2)
C15A—O6A—C14A—C17A	−152.68 (17)	C2C—O1C—C1C—C5C	−152.21 (18)
C15A—O6A—C14A—C18A	82.1 (2)	C2C—C3C—C6C—O3C	−43.2 (2)
C16A—O5A—C14A—O6A	32.5 (2)	C2C—C3C—C6C—C10C	79.0 (2)
C16A—O5A—C14A—C17A	148.07 (17)	C3C—O2C—C1C—O1C	33.7 (2)
C16A—O5A—C14A—C18A	−87.3 (2)	C3C—O2C—C1C—C4C	−85.8 (2)
O1B—C2B—C3B—O2B	6.1 (2)	C3C—O2C—C1C—C5C	149.6 (2)
O1B—C2B—C3B—C6B	124.74 (18)	C3C—C6C—C10C—O4C	−60.68 (19)
O2B—C3B—C6B—O3B	74.95 (19)	C3C—C6C—C10C—C16C	175.45 (15)
O2B—C3B—C6B—C10B	−163.43 (16)	C6C—O3C—C7C—C8C	−75.3 (2)
O3B—C6B—C10B—O4B	62.37 (18)	C6C—C10C—C16C—O5C	−170.65 (15)
O3B—C6B—C10B—C16B	−61.4 (2)	C6C—C10C—C16C—C15C	73.3 (2)
O4B—C10B—C16B—O5B	67.6 (2)	C7C—O3C—C6C—C3C	−88.57 (19)
O4B—C10B—C16B—C15B	−48.5 (2)	C7C—O3C—C6C—C10C	147.38 (16)
O6B—C15B—C16B—O5B	30.37 (19)	C10C—O4C—C11C—C12C	−88.7 (2)
O6B—C15B—C16B—C10B	148.86 (16)	C11C—O4C—C10C—C6C	140.16 (17)
C1B—O1B—C2B—C3B	15.7 (2)	C11C—O4C—C10C—C16C	−94.69 (19)
C1B—O2B—C3B—C2B	−25.8 (2)	C14C—O5C—C16C—C10C	−136.98 (16)
C1B—O2B—C3B—C6B	−149.86 (18)	C14C—O5C—C16C—C15C	−12.4 (2)

C2B—O1B—C1B—O2B	−32.1 (2)	C14C—O6C—C15C—C16C	−36.9 (2)
C2B—O1B—C1B—C4B	87.8 (2)	C15C—O6C—C14C—O5C	29.9 (2)
C2B—O1B—C1B—C5B	−146.99 (19)	C15C—O6C—C14C—C17C	−88.8 (2)
C2B—C3B—C6B—O3B	−41.0 (2)	C15C—O6C—C14C—C18C	146.37 (19)
C2B—C3B—C6B—C10B	80.6 (2)	C16C—O5C—C14C—O6C	−10.0 (2)
C3B—O2B—C1B—O1B	36.2 (2)	C16C—O5C—C14C—C17C	109.8 (2)
C3B—O2B—C1B—C4B	−83.7 (2)	C16C—O5C—C14C—C18C	−125.87 (19)

Hydrogen-bond geometry (Å, º)

D—H···*A*	*D*—H	H···*A*	*D*···*A*	*D*—H···*A*
C7*A*—H7*AA*···O1*B*^{i}	0.99	2.55	3.393 (3)	143
C9*A*—H9*A*···O6*C*^{ii}	0.95	2.58	3.375 (3)	141
C13*A*—H13*A*···O6*A*^{iii}	0.95	2.34	3.246 (3)	158
C18*A*—H18*B*···O5*C*^{iv}	0.98	2.62	3.581 (3)	168
C5*B*—H5*BA*···O3*A*^{v}	0.98	2.59	3.525 (3)	160
C9*B*—H9*B*···O3*C*	0.95	2.19	3.121 (3)	167
C13*B*—H13*B*···O6*B*^{iii}	0.95	2.21	3.138 (3)	165
C16*B*—H16*B*···O1*C*	1.00	2.69	3.584 (2)	149
C4*C*—H4*CB*···O2*A*^{vi}	0.98	2.57	3.536 (3)	169
C6*C*—H6*C*···O5*A*^{vi}	1.00	2.67	3.458 (2)	136
C9*C*—H9*C*···O2*A*^{vii}	0.95	2.71	3.542 (3)	147
C11*C*—H11*E*···O2*B*^{viii}	0.99	2.38	3.372 (3)	177
C13*C*—H13*C*···O6*C*^{ix}	0.95	2.34	3.278 (3)	168

Symmetry codes: (i) *x*−1, *y*−1, *z*; (ii) *x*, *y*−1, *z*−1; (iii) *x*+1, *y*, *z*; (iv) *x*, *y*, *z*−1; (v) *x*+1, *y*+1, *z*; (vi) *x*, *y*, *z*+1; (vii) *x*, *y*+1, *z*+1; (viii) *x*−1, *y*, *z*; (ix) *x*, *y*−1, *z*.